Int. J. Appl. Comput. Math (2022) 8:188
https://doi.org/10.1007/s40819-022-01408-z

ORIGINAL PAPER

Numerical Solution of Two-Dimensional Time Fractional Mobile/Immobile Equation Using Explicit Group Methods

Fouad Mohammad Salama[1] · **Umair Ali**[2] · **Ajmal Ali**[3]

Accepted: 4 July 2022 / Published online: 15 July 2022

Abstract
In this paper, we shall present the development of two explicit group schemes, namely, fractional explicit group (FEG) and modified fractional explicit group (MFEG) methods for solving the time fractional mobile/immobile equation in two space dimensions. The presented methods are formulated based on two Crank-Nicolson (C-N) finite difference schemes established at two different grid spacings. The stability and convergence of order $O(\tau^{2-\alpha} + h^2)$ are rigorously proven using Fourier analysis. Several numerical experiments are conducted to verify the efficiency of the proposed methods. Meanwhile, numerical results show that the FEG and MFEG algorithms are able to reduce the computational times and iterations effectively while preserving good accuracy in comparison to the C-N finite difference method.

Keywords Fractional mobile/immobile equation · Grouping strategy · Crank-Nicolson finite difference · Stability · Convergence · Numerical experiments

Mathematics Subject Classification 35R11, 65N06, 65N12

Introduction

The roots of fractional calculus are nearly as old as those of classical calculus. However, it was only at the turn of the century that interest in fractional calculus exploded. In accordance with this, the first book along with the first conference on fractional calculus and its applications did not appear until 1974. For some researchers, this year is viewed as the beginning of a new era for fractional calculus. Nowdays, a large number of research articles and books are devoted to this topic, and its applications in various areas such as physics, biology, chemistry, finance and economy are witnessing remarkable progress, see [1–11] and the

U. Ali, A. Ali: These authors contributed equally to this work.

✉ Fouad Mohammad Salama
fuadmohd321@gmail.com

[1] School of Mathematical Sciences, Universiti Sains Malaysia, 11800 Gelugor, Penang, Malaysia

[2] Department of Applied Mathematics and Statistics, Institute of Space Technology, 44000 Islamabad, Islamabad, Pakistan

[3] Department of Mathematics, Virtual University of Pakistan, 54000 Lahore, Lahore, Pakistan

references therein. The popularity of fractional calculus in all branches of science stems from its successful application in modelling physical phenomena, specifically in the form of fractional differential equations. For instance, Zhang et al. [12] introduced an image enhancement approach for single-pixel imaging that is based on fractional order operators. The authors argue that the new fractional approach strikes a good balance between edge detection and noise suppression, making it useful in areas such as feature extraction and object recognition, in addition to military and industrial applications. Aman et al. [13] considered some fractional-order PDEs to study the memory properties pertaining to the behavior of nanofluids, which cannot be addressed by integer-order PDEs. The authors mentioned that their work has useful applications in diverse fields such as physics, engineering and many others. Khan et al. [14] extended the classical Maxwell equation to its counterpart fractional-order Maxwell model via the emerging definition of the Caputo-Fabrizio derivative. The resulting fractional model was then applied to account for the heat transfer due to convection occurring in a generalized Maxwell fluid. Almeida et al. [15] scrutinized two mathematical models namely, the population growth model and the gross domestic product model, by using fractional differential equations described in the frame of Caputo derivative with respect to another function. Alshabanat et al. [16] generalized the concept of the Caputo-Fabrizio fractional derivative and provided some applications to RC-electrical circuits on the basis of fractional differential equations involving the new developed definition. With the help of a fractional-order model, Ali et al. [17] discussed the flow of Jeffrey nanofluid under the effects of thermal radiation and heat/mass transfer. The governing fractional differential equation was described in the Atangana-Baleanu sense. In [18], two epidemic fractional models for describing infection dynamics together with a macroeconomic fractional model were investigated numerically. Uçar et al. [19] yielded approximate numerical solutions for the giving up smoking model expressed in terms of the Atangana-Baleanu fractional differential equation. In another study, Alrabaiah et al. [20] dealt with the phenomenon of tobacco smoking with snuffing class via a system of Caputo-type fractional differential equations. Ndaïrou et al. [21] reported on the mathematical and numerical analysis of a fractional Caputo differential system that approximates the infectious individuals of COVID-19. Some other valuable work on the application of fractional calculus can be found in [22–25].

This article focuses on developing explicit group schemes for the two-dimensional time fractional mobile/immobile equation of the following form:

$$\frac{\partial u}{\partial t} + {}_0^C D_t^\alpha u = \Delta u + f(x, y, t), \quad (x, y, t) \in \Omega \times (0, T], \tag{1}$$

subject to the initial and boundary conditions

$$u(x, y, 0) = g(x, y), \quad (x, y) \in \Omega \tag{2}$$

$$u(x, y, t) = \phi(x, y, t), \quad (x, y, t) \in \partial\Omega \times (0, T], \tag{3}$$

where $\Delta = \frac{\partial^2}{\partial x^2} + \frac{\partial^2}{\partial y^2}$ is the Laplacian operator, $f(x, y, t)$, $\phi(x, y, t)$ and $g(x, y)$ are given smooth functions. $\Omega = \{(x, y)|0 < x < L,\ 0 < y < L\}$ and $\partial\Omega$ is its boundary. ${}_0^C D_t^\alpha$ ($\alpha \in (0, 1)$) represents the Caputo fractional derivative defined by

$${}_0^C D_t^\alpha u(x, y, t) = \frac{1}{\Gamma(1-\alpha)} \int_0^t (t-\xi)^{-\alpha} \frac{\partial u(x, y, \xi)}{\partial \xi} d\xi.$$

The time fractional mobile/immobile Eq. (1) plays a central role in describing various phenomena including heat diffusion and propagation of ocean sounds, among others. Moreover,

it has been verified that the long term limit of continuous time random walks can be controlled by the fractional mobile/immobile equation [26], which interprets the probabilistic nature of the latter. In most cases, fractional partial differential equations (PDEs) are difficult to deal with analytically, and therefore, numerical or approximate analytical solutions become indispensable. In the following, we present some recent numerical developments in solving fractional mobile/immobile equations. Liu and Li [27] presented a Crank-Nicolson (C-N) difference scheme for the one-dimensional mobile/immobile equation with time derivative of variable order. Pourbashash et al. [28] proposed a compact difference scheme for solving the one-dimensional time fractional mobile/immobile equation. The stability and convergence of the numerical scheme were proved using Fourier method. Qiu et al. [29] developed a time two-grid method based on a finite difference approach for the nonlinear time fractional mobile/immobile equation in two dimensions. Yang et al. [26] developed the C-N orthogonal spline collocation method for the two-dimensional time fractional mobile/immobile equation. Jiang et al. [30] considered an alternating direction implict (ADI) compact scheme to solve the semilinear time fractional mobile/immobile equation in two dimensions. Yin et al. [31] employed the generalized BDF2-θ technique in time and finite element in space to deal with the two-dimensional mobile/immobile equation with Riemann-Liouville time derivative. In addition, Chai et al. [32] constructed the high order compact difference schemes for the one-dimensional and two-dimensional time fractional mobile/immobile equations.

Generally speaking, numerical methods for fractional PDEs are abundant, whereas efficient numerical methods leading to rapid convergence, particularly for time fractional mobile/immobile equations, are relatively sparse. This motivates us to develop fast numerical schemes to solve them. This is useful for long time simulations, especially when attempting to solve multi-dimensional fractional problems [33–36]. It is well known that explicit group methods can diminish the computational complexity and reduce the computational time of numerical algorithms effectively [37–44]. However, numerical approximations based on explicit group methods for fractional mobile/immobile equations are still at an early stage of development. The main goal of this paper is to construct two fractional explicit group methods based on C-N difference schemes for solving Eq. (1). The stability in l^2 norm and the convergence order $O(\tau^{2-\alpha}+h^2)$, where τ and h are respectively the temporal and spatial step sizes, will be proved. Numerical experiments to show that the proposed methods are more efficient than the C-N difference method in terms of execution time are also provided.

The outline of this paper is as follows. Section 2 devotes to the derivation of the C-N finite difference scheme. In Sect. 3, the fractional explicit group methods are constructed. The stability and convergence are rigorously proved in Sects. 4 and 5, respectively. In Sect. 6, some numerical simulations are carried out by using the C-N scheme and the two fractional explicit group methods, and some comparisons between three methods are demonstrated. Finally, a brief summary is given in Sect. 7.

The C-N Difference Scheme

In order to discretize the solution domain, we define $\Omega_{\Delta x,\Delta y}=\{(x_i,y_j)|x_i=i\Delta x,\ y_j=j\Delta y,\ \Delta x=L/M_x,\ \Delta y=L/M_y,\ 0\le i\le M_x, 0\le j\le M_y\}$ to be a uniform mesh of domain Ω. Likewise, define $\Omega_\tau=\{t_k,\ t_k=k\tau,\ \tau=T/N,\ 0\le k\le N\}$ to be a uniform mesh of interval $[0,T]$. M_x, M_y and N are positive integers. Let $u_{i,j}^k$ be the solution value at the grid point (x_i,y_j,t_k). Then, the C-N approximation to Eq. (1) can be expressed as

follows:

$$\left.\frac{\partial u}{\partial t}\right|_{i,j}^{k+1/2} + \left.\frac{\partial^{\alpha} u}{\partial t^{\alpha}}\right|_{i,j}^{k+1/2} = \left.\frac{\partial^2 u}{\partial x^2}\right|_{i,j}^{k+1/2} + \left.\frac{\partial^2 u}{\partial y^2}\right|_{i,j}^{k+1/2} + f_{i,j}^{k+1/2}. \tag{4}$$

A discrete approximation to the Caputo time fractional derivative ${}_0^C D_t^{\alpha} u(x, y, t)$ is given by the formula [45, 46]

$$\left.\frac{\partial^{\alpha} u}{\partial t^{\alpha}}\right|_{i,j}^{k+1/2} = \left[W_1 u_{i,j}^{k} + \sum_{m=1}^{k-1} \left(W_{k-m+1} - W_{k-m}\right) u_{i,j}^{m} - W_k u_{i,j}^{0} + \sigma \frac{\left(u_{i,j}^{k+1} - u_{i,j}^{k}\right)}{2^{1-\alpha}} \right] + O(\tau^{2-\alpha}), \tag{5}$$

where

$$\sigma = \frac{1}{\Gamma(2-\alpha)\tau^{\alpha}}, \; W_n = \sigma\left((n+1/2)^{1-\alpha} - (n-1/2)^{1-\alpha}\right).$$

In addition, utilizing Taylor expansion, we have

$$\left.\frac{\partial^2 u}{\partial x^2}\right|_{i,j}^{k+1/2} = \frac{1}{2}\left[\frac{u_{i+1,j}^{k+1} - 2u_{i,j}^{k+1} + u_{i-1,j}^{k+1}}{(\Delta x)^2} + \frac{u_{i+1,j}^{k} - 2u_{i,j}^{k} + u_{i-1,j}^{k}}{(\Delta x)^2} \right] + O(\tau^2 + (\Delta x)^2) + (\Delta y)^2), \tag{6}$$

$$\left.\frac{\partial^2 u}{\partial y^2}\right|_{i,j}^{k+1/2} = \frac{1}{2}\left[\frac{u_{i,j+1}^{k+1} - 2u_{i,j}^{k+1} + u_{i,j-1}^{k+1}}{(\Delta x)^2} + \frac{u_{i,j+1}^{k} - 2u_{i,j}^{k} + u_{i,j-1}^{k}}{(\Delta x)^2} \right] + O(\tau^2 + (\Delta x)^2) + (\Delta y)^2), \tag{7}$$

and

$$\left.\frac{\partial u}{\partial t}\right|_{i,j}^{k+1/2} = \frac{u_{i,j}^{k+1} - u_{i,j}^{k}}{2} + O(\tau^2). \tag{8}$$

Substituting (5-8) into (4), we obtain the following difference equation

$$\begin{aligned} &\frac{u_{i,j}^{k+1} - u_{i,j}^{k}}{\tau} + W_1 u_{i,j}^{k} + \sum_{m=1}^{k-1} \left(W_{k-m+1} - W_{k-m}\right) u_{i,j}^{m} - W_k u_{i,j}^{0} + \sigma\left(\frac{u_{i,j}^{k+1} - u_{i,j}^{k}}{2^{1-\alpha}}\right) \\ &= \frac{1}{2}\left[\frac{u_{i+1,j}^{k+1} - 2u_{i,j}^{k+1} + u_{i-1,j}^{k+1}}{h^2} + \frac{u_{i+1,j}^{k} - 2u_{i,j}^{k} + u_{i-1,j}^{k}}{h^2} \right] \\ &+ \frac{1}{2}\left[\frac{u_{i,j+1}^{k+1} - 2u_{i,j}^{k+1} + u_{i,j-1}^{k+1}}{h^2} + \frac{u_{i,j+1}^{k} - 2u_{i,j}^{k} + u_{i,j-1}^{k}}{h^2} \right] \\ &+ f_{i,j}^{k+1/2} + O(\tau^{2-\alpha} + h^2), \end{aligned} \tag{9}$$

in which $h = \Delta x = \Delta y$. By disregarding the higher order term in the above equation and replacing $u_{i,j}^{k}$ with its numerical approximation $U_{i,j}^{k}$, the following C-N difference scheme is obtained

$$\begin{aligned} (1 + 4H_1 + H_2)U_{i,j}^{k+1} = {} & H_1(U_{i+1,j}^{k+1} + U_{i-1,j}^{k+1} + U_{i+1,j}^{k} + U_{i-1,j}^{k}) + H_1(U_{i,j+1}^{k+1} + U_{i,j-1}^{k+1} \\ & + U_{i,j+1}^{k} + U_{i,j-1}^{k}) + (1 - \tau W_1 - 4H_1 + H_2)U_{i,j}^{k} \end{aligned}$$

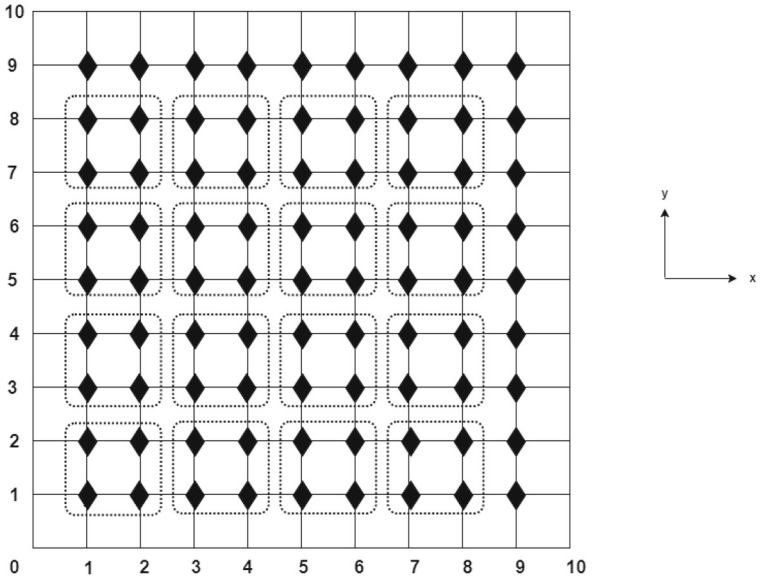

Fig. 1 Grouping of mesh points for the FEG method with $M_x = M_y = 10$

$$+\tau\sum_{m=1}^{k-1}(W_{k-m}-W_{k-m+1})\,U_{i,j}^{m}+\tau W_k U_{i,j}^{0}+\tau f_{i,j}^{k+1/2}, \qquad (10)$$

where $H_1 = \frac{\tau}{2h^2}$ and $H_2 = \frac{\tau\sigma}{2^{1-\alpha}}$.

Formulation of Group Methods

The Fractional Explicit Group (FEG) Method

Consider the C-N difference scheme (10). Let the mesh points be grouped in blocks of four points as shown in Fig. 1. Then, Eq. (10) is applied to any group of four points so that the following (4×4) system of equations is obtained

$$\begin{pmatrix} Q & -H_1 & 0 & -H_1 \\ -H_1 & Q & -H_1 & 0 \\ 0 & -H_1 & Q & -H_1 \\ -H_1 & 0 & -H_1 & Q \end{pmatrix} \begin{pmatrix} U_{i,j}^{k+1} \\ U_{i+1,j}^{k+1} \\ U_{i+1,j+1}^{k+1} \\ U_{i,j+1}^{k+1} \end{pmatrix} = \begin{pmatrix} rhs_{i,j} \\ rhs_{i+1,j} \\ rhs_{i+1,j+1} \\ rhs_{i,j+1} \end{pmatrix}, \qquad (11)$$

where $Q = 1 + 4H_1 + H_2$,

$$\begin{aligned} rhs_{i,j} &= H_1(U_{i-1,j}^{k+1} + U_{i+1,j}^{k} + U_{i-1,j}^{k}) + H_1(U_{i,j-1}^{k+1} + U_{i,j+1}^{k} + U_{i,j-1}^{k}) \\ &\quad + (1 - \tau W_1 - 4H_1 + H_2)U_{i,j}^{k} + \tau\sum_{m=1}^{k-1}(W_{k-m} - W_{k-m+1})\,U_{i,j}^{m} \\ &\quad + \tau W_k U_{i,j}^{0} + \tau f_{i,j}^{k+1/2}, \end{aligned}$$

$$
\begin{aligned}
rhs_{i+1,j} &= H_1(U^{k+1}_{i+2,j} + U^{k}_{i+2,j} + U^{k}_{i,j}) + H_1(U^{k+1}_{i+1,j-1} + U^{k}_{i+1,j+1} + U^{k}_{i+1,j-1}) \\
&\quad + (1 - \tau W_1 - 4H_1 + H_2)U^{k}_{i+1,j} + \tau \sum_{m=1}^{k-1} (W_{k-m} - W_{k-m+1})\, U^{m}_{i+1,j} \\
&\quad + \tau W_k U^{0}_{i+1,j} + \tau f^{k+1/2}_{i+1,j}, \\
rhs_{i+1,j+1} &= H_1(U^{k+1}_{i+2,j+1} + U^{k}_{i+2,j+1} + U^{k}_{i,j+1}) + H_1(U^{k+1}_{i+1,j+2} + U^{k}_{i+1,j+2} + U^{k}_{i+1,j}) \\
&\quad + (1 - \tau W_1 - 4H_1 + H_2)U^{k}_{i+1,j+1} + \tau \sum_{m=1}^{k-1} (W_{k-m} - W_{k-m+1})\, U^{m}_{i+1,j+1} \\
&\quad + \tau W_k U^{0}_{i+1,j+1} + \tau f^{k+1/2}_{i+1,j+1}, \\
rhs_{i,j+1} &= H_1(U^{k+1}_{i-1,j+1} + U^{k}_{i+1,j+1} + U^{k}_{i-1,j+1}) + H_1(U^{k+1}_{i,j+2} + U^{k}_{i,j+2} + U^{k}_{i,j}) \\
&\quad + (1 - \tau W_1 - 4H_1 + H_2)U^{k}_{i,j+1} + \tau \sum_{m=1}^{k-1} (W_{k-m} - W_{k-m+1})\, U^{m}_{i,j+1} \\
&\quad + \tau W_k U^{0}_{i,j+1} + \tau f^{k+1/2}_{i,j+1}.
\end{aligned}
$$

The coefficients matrix in 11 can be inverted to get the four-point FEG equation

$$
\begin{pmatrix} U^{k+1}_{i,j} \\ U^{k+1}_{i+1,j} \\ U^{k+1}_{i+1,j+1} \\ U^{k+1}_{i,j+1} \end{pmatrix} = \begin{pmatrix} A_1 & A_2 & A_3 & A_2 \\ A_2 & A_1 & A_2 & A_3 \\ A_3 & A_2 & A_1 & A_2 \\ A_2 & A_3 & A_2 & A_1 \end{pmatrix} \begin{pmatrix} rhs_{i,j} \\ rhs_{i+1,j} \\ rhs_{i+1,j+1} \\ rhs_{i,j+1} \end{pmatrix}, \tag{12}
$$

where

$$
\begin{aligned}
A_1 &= \frac{14H_1^2 + 8H_1H_2 + H_2^2 + 8H_1 + 8H_2 + 1}{(2H_1 + H_2 + 1)(6H_1 + H_2 + 1)(1 + 4H_1 + H_2)} \\
A_2 &= \frac{H_1}{(2H_1 + H_2 + 1)(6H_1 + H_2 + 1)}, \\
A_3 &= \frac{2H_1^2}{(2H_1 + H_2 + 1)(6H_1 + H_2 + 1)(4H_1 + H_2 + 1)}.
\end{aligned}
$$

Figure 1 depicts the grouping of mesh points into blocks of four points with mesh size $M_x = M_y = 10$. It is obvious that the execution of Eq. (12) is only applicable for the grouped points. Therefore, the implementation of the FEG method is carried out by applying Eq. (12) to each group in Fig. 1. Before moving to the next time level, we calculate the remaining ungrouped points near the boundaries by utilizing Eq. (10). At each time level, the computation process is carried out in an iterative manner until the final time level N is reached. For convenience, the FEG method is defined in Algorithm 1.

Algorithm 1 Solution algorithm using the FEG iterative method

1. Divide the grid points of the discretized solution domain into groups of four points as shown in Fig. 1.
2. Use Eq. (12) to iterate the solutions at all grouped points ♦ at time level $k+1$.
3. Use Eq. (10) to iterate the solutions at the ungrouped points ♦ near the right and top boundaries.
4. Test the convergence. If the iterative solutions converge, move to the next time level. Otherwise, repeat the iteration process at the same time level in steps 2 and 3.
5. Once the targeted time level is reached, print the numerical results.

The Modified Fractional Explicit Group (MFEG) Method

Another approximation scheme for Eq. (1) is obtained by Taylor's expansion and considering points at mesh size of $2h$. The C-N difference scheme with $2h$ spacing is as follows

$$\begin{aligned}
&\frac{u_{i,j}^{k+1}-u_{i,j}^{k}}{\tau}+W_1u_{i,j}^{k}+\sum_{m=1}^{k-1}\left(W_{k-m+1}-W_{k-m}\right)u_{i,j}^{m}-W_ku_{i,j}^{0}+\sigma\left(\frac{u_{i,j}^{k+1}-u_{i,j}^{k}}{2^{1-\alpha}}\right)\\
&=\frac{1}{2}\left[\frac{u_{i+2,j}^{k+1}-2u_{i,j}^{k+1}+u_{i-2,j}^{k+1}}{4h^2}+\frac{u_{i+2,j}^{k}-2u_{i,j}^{k}+u_{i-2,j}^{k}}{4h^2}\right]\\
&\quad+\frac{1}{2}\left[\frac{u_{i,j+2}^{k+1}-2u_{i,j}^{k+1}+u_{i,j-2}^{k+1}}{4h^2}+\frac{u_{i,j+2}^{k}-2u_{i,j}^{k}+u_{i,j-2}^{k}}{4h^2}\right]\\
&\quad+f_{i,j}^{k+1/2}+O(\tau^{2-\alpha}+h^2),
\end{aligned}\tag{13}$$

On simplification with $U_{i,j}^{k}$ being the numerical approximation of $u_{i,j}^{k}$, the following equation is obtained

$$\begin{aligned}
(1+4G_1+G_2)U_{i,j}^{k+1}&=G_1(U_{i+2,j}^{k+1}+U_{i-2,j}^{k+1}+U_{i+2,j}^{k}+U_{i-2,j}^{k})+G_1(U_{i,j+2}^{k+1}+U_{i,j-2}^{k+1}\\
&\quad+U_{i,j+2}^{k}+U_{i,j-2}^{k})+(1-\tau W_1-4G_1+G_2)U_{i,j}^{k}\\
&\quad+\tau\sum_{m=1}^{k-1}\left(W_{k-m}-W_{k-m+1}\right)U_{i,j}^{m}+\tau W_kU_{i,j}^{0}+\tau f_{i,j}^{k+1/2},
\end{aligned}\tag{14}$$

where $G_1=\frac{\tau}{8h^2}$ and $G_2=\frac{\tau\sigma}{2^{1-\alpha}}$.
Now applying the C-N difference formula with $2h$ spacing (14) to any group of four points will lead to the following (4×4) system

$$\begin{pmatrix} S & -G_1 & 0 & -G_1\\ -G_1 & S & -G_1 & 0\\ 0 & -G_1 & S & -G_1\\ -G_1 & 0 & -G_1 & S \end{pmatrix}\begin{pmatrix} U_{i,j}^{k+1}\\ U_{i+2,j}^{k+1}\\ U_{i+2,j+2}^{k+1}\\ U_{i,j+2}^{k+1}\end{pmatrix}=\begin{pmatrix} rhs_{i,j}\\ rhs_{i+2,j}\\ rhs_{i+2,j+2}\\ rhs_{i,j+2}\end{pmatrix},\tag{15}$$

where $S=1+4G_1+G_2$,

$$\begin{aligned}
rhs_{i,j}&=G_1(U_{i-2,j}^{k+1}+U_{i+2,j}^{k}+U_{i-2,j}^{k})+G_1(U_{i,j-2}^{k+1}+U_{i,j+2}^{k}+U_{i,j-2}^{k})\\
&\quad+(1-\tau W_1-4G_1+G_2)U_{i,j}^{k}+\tau\sum_{m=1}^{k-1}\left(W_{k-m}-W_{k-m+1}\right)U_{i,j}^{m}\\
&\quad+\tau W_kU_{i,j}^{0}+\tau f_{i,j}^{k+1/2},\\
rhs_{i+2,j}&=G_1(U_{i+4,j}^{k+1}+U_{i+4,j}^{k}+U_{i,j}^{k})+G_1(U_{i+2,j-2}^{k+1}+U_{i+2,j+2}^{k}+U_{i+2,j-2}^{k})
\end{aligned}$$

$$
\begin{aligned}
&+ (1 - \tau W_1 - 4G_1 + G_2)U^k_{i+2,j} + \tau \sum_{m=1}^{k-1} (W_{k-m} - W_{k-m+1})\, U^m_{i+2,j} \\
&+ \tau W_k U^0_{i+2,j} + \tau f^{k+1/2}_{i+2,j}, \\
rhs_{i+2,j+2} &= G_1(U^{k+1}_{i+4,j+2} + U^k_{i+4,j+2} + U^k_{i,j+2}) + G_1(U^{k+1}_{i+2,j+4} + U^k_{i+2,j+4} + U^k_{i+2,j}) \\
&+ (1 - \tau W_1 - 4G_1 + G_2)U^k_{i+2,j+2} + \tau \sum_{m=1}^{k-1} (W_{k-m} - W_{k-m+1})\, U^m_{i+2,j+2} \\
&+ \tau W_k U^0_{i+2,j+2} + \tau f^{k+1/2}_{i+2,j+2}, \\
rhs_{i,j+2} &= G_1(U^{k+1}_{i-2,j+2} + U^k_{i+2,j+2} + U^k_{i-2,j+2}) + G_1(U^{k+1}_{i,j+4} + U^k_{i,j+4} + U^k_{i,j}) \\
&+ (1 - \tau W_1 - 4G_1 + G_2)U^k_{i,j+2} + \tau \sum_{m=1}^{k-1} (W_{k-m} - W_{k-m+1})\, U^m_{i,j+2} \\
&+ \tau W_k U^0_{i,j+2} + \tau f^{k+1/2}_{i,j+2}.
\end{aligned}
$$

The above system can be rewritten in explicit form which results in the four-point MFEG equation

$$
\begin{pmatrix} U^{k+1}_{i,j} \\ U^{k+1}_{i+2,j} \\ U^{k+1}_{i+2,j+2} \\ U^{k+1}_{i,j+2} \end{pmatrix} = \begin{pmatrix} B_1 & B_2 & B_3 & B_2 \\ B_2 & B_1 & B_2 & B_3 \\ B_3 & B_2 & B_1 & B_2 \\ B_2 & B_3 & B_2 & B_1 \end{pmatrix} \begin{pmatrix} rhs_{i,j} \\ rhs_{i+2,j} \\ rhs_{i+2,j+2} \\ rhs_{i,j+2} \end{pmatrix}, \tag{16}
$$

where

$$
\begin{aligned}
B_1 &= \frac{14G_1^2 + 8G_1G_2 + G_2^2 + 8G_1 + 8G_2 + 1}{(2G_1 + G_2 + 1)(6G_1 + G_2 + 1)(1 + 4G_1 + G_2)} \\
B_2 &= \frac{G_1}{(2G_1 + G_2 + 1)(6G_1 + G_2 + 1)}, \\
B_3 &= \frac{2G_1^2}{(2G_1 + G_2 + 1)(6G_1 + G_2 + 1)(4G_1 + G_2 + 1)}.
\end{aligned}
$$

In the MFEG method, the mesh points of the discretized solution domain Ω are arranged into several groups. Each group comprise four points of type ♦ (shown in Fig. 2). The MFEG Eq. (16) is applied to generate iterations on each group in Fig. 2. Prior going to the next time level, the remaining points of the mesh (□ and ○) can be obtained directly once utilizing the following sequence:

1. The skewed C-N difference formula obtained by rotating the $x - y$ axis 45° clockwise is used for □ points. With $K_1 = \tau/4h^2$ and $K_2 = (\tau\sigma)/2^{1-\alpha}$, the skewed C-N difference scheme for Eq. (1) is given by

$$
\begin{aligned}
&(1 + 4K_1 + K_2)U^{k+1}_{i,j} \\
&= K_1(U^{k+1}_{i+1,j-1} + U^{k+1}_{i-1,j+1} + U^k_{i+1,j-1} + U^k_{i-1,j+1}) + K_1(U^{k+1}_{i+1,j+1} \\
&\quad + U^{k+1}_{i-1,j-1} + U^k_{i+1,j+1} + U^k_{i-1,j-1}) + (1 - \tau W_1 - 4K_1 + K_2)U^k_{i,j} \\
&\quad + \tau \sum_{m=1}^{k-1} (W_{k-m} - W_{k-m+1})\, U^m_{i,j} + \tau W_k U^0_{i,j} + \tau f^{k+1/2}_{i,j},
\end{aligned} \tag{17}
$$

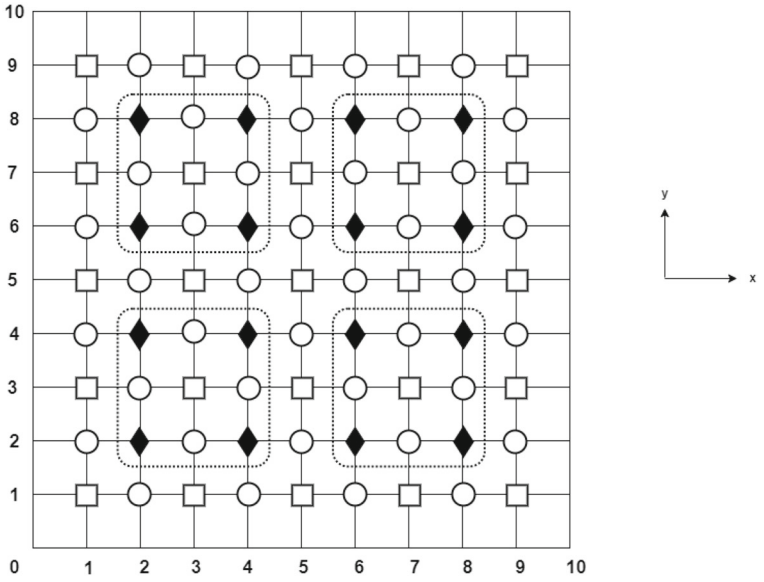

Fig. 2 Grouping of mesh points for the MFEG method with $M_x = M_y = 10$

2. The C-N difference formula (10) is utilized for ○ points.

The MFEG method is illustrated in Algorithm 2. From the described solution procedure, it may be observed that the MFEG method involves only a quarter of the mesh points in the iterative process at each time level. Due to this reduction of points that take part in the iterative process, the MFEG method is expected to save more CPU time in solving Eq. (1).

Algorithm 2 Solution algorithm using the MFEG iterative method

1. Divide the grid points of the discretized solution domain into three types ♦, ○ and □ as depicted in Fig. 2.
2. Arrange all the ♦ points into group of four points.
3. Use Eq. (16) to iterate the solutions at the grouped points ♦ at time level $k + 1$.
4. Test the convergence. If the iterative solutions converge, move to step 5. Otherwise, repeat the iteration process at the same time level in step 3.
5. The solutions at the residual grid points □ and ○ are computed directly once as follows:
   (a) Use Eq. (17) to compute the solutions at the points of type □.
   (b) For the residual points of type ○, Eq. (10) is employed.
6. Once the targeted time level is reached, print the numerical results.

Stability Analysis

This section is devoted to the stability of the C-N difference schemes (10) and (14), which are the basis of the FEG and MFEG methods, respectively. The following lemma is introduced for the convenience of our analysis

Lemma 1 *The coefficients W_n in Eq. (14) satisfy*

1. $W_{k-m} > W_{k-m+1}, \quad m = 0, 1, 2, \ldots, k-1.$
2. $\sum_{m=1}^{k-1} (W_{k-m} - W_{k-m+1}) = W_1 - W_k.$

Stability of the *h*-Spaced C-N Numerical Scheme

Let $\hat{U}_{i,j}^k$ be the approximate solution of (10), and define

$$\vartheta_{i,j}^k = U_{i,j}^k - \hat{U}_{i,j}^k, \tag{18}$$

Then by setting (18) into (10), we get

$$\begin{aligned}(1+4H_1+H_2)\vartheta_{i,j}^{k+1} - H_1(\vartheta_{i+1,j}^{k+1}+\vartheta_{i-1,j}^{k+1}) - H_1(\vartheta_{i,j+1}^{k+1}+\vartheta_{i,j-1}^{k+1})\\ = (1-\tau W_1 - 4H_1 + H_2)\vartheta_{i,j}^k + H_1(\vartheta_{i+1,j}^k+\vartheta_{i-1,j}^k) + H_1(\vartheta_{i,j+1}^k+\vartheta_{i,j-1}^k)\\ + \tau\sum_{m=1}^{k-1}(W_{k-m}-W_{k-m+1})\,\vartheta_{i,j}^m + \tau W_k\vartheta_{i,j}^0.\end{aligned} \tag{19}$$

The Fourier series for $\vartheta^k(x,y)$ is

$$\vartheta^k(x,y) = \sum_{Z_1=-\infty}^{\infty}\sum_{Z_2=-\infty}^{\infty}\lambda^k(Z_1,Z_2)e^{2\pi I(Z_1x/L+Z_2y/L)},$$

where $I=\sqrt{-1}$ and the Fourier coefficients $\lambda^k(Z_1,Z_2)$ is given by

$$\lambda^k(Z_1,Z_2) = \frac{1}{L^2}\int_0^L\int_0^L \vartheta^k(x,y)e^{-2\pi I(Z_1x/L+Z_2y/L)}dxdy, \tag{20}$$

Introducing the following norm

$$\|\vartheta^k\|_2 = \left(\sum_{j=1}^{M_y-1}\sum_{i=1}^{M_x-1}\Delta y\Delta x|\vartheta_{i,j}^k|^2\right)^{1/2} = \left(\int_0^L\int_0^L|\vartheta_{i,j}^k|^2dxdy\right)^{1/2}.$$

Applying the Parseval's equality

$$\int_0^L\int_0^L|\vartheta_{i,j}^k|^2dxdy = \sum_{Z_2=-\infty}^{\infty}\sum_{Z_1=-\infty}^{\infty}|\lambda^k(Z_1,Z_2)|^2,$$

we get

$$\|\vartheta^k\|_2 = \left(\sum_{Z_2=-\infty}^{\infty}\sum_{Z_1=-\infty}^{\infty}|\lambda^k(Z_1,Z_2)|^2\right)^{1/2}, \tag{21}$$

With $\gamma_1 = 2\pi Z_1/L$ and $\gamma_2 = 2\pi Z_2/L$, and based on the above analysis, we assume that the solutions of Eq. (19) is of the following form

$$\vartheta_{i,j}^k = \lambda^k e^{I(\gamma_1 i\Delta x+\gamma_2 j\Delta y)}. \tag{22}$$

Lemma 2 *Suppose* λ^k *is defined by* (20)*. If* $2+2H_2-2\tau W_1 \geq 0$*, then we have*

$$|\lambda^{k+1}| \leq |\lambda^0|, \quad k=0,1,2,\ldots,N-1.$$

Proof Setting $\vartheta_{i,j}^k = \lambda^k e^{I(\gamma_1 i\Delta x+\gamma_2 j\Delta y)}$ into Eq. (19), we obtain

$$\begin{aligned}(1+4H_1+H_2)\lambda^{k+1}e^{I(\gamma_1 i\Delta x+\gamma_2 j\Delta y)} - H_1\lambda^{k+1}(e^{I(\gamma_1(i+1)\Delta x+\gamma_2 j\Delta y)}\\ + e^{I(\gamma_1(i-1)\Delta x+\gamma_2 j\Delta y)}) - H_1\lambda^{k+1}(e^{I(\gamma_1 i\Delta x+\gamma_2(j+1)\Delta y)} + e^{I(\gamma_1 i\Delta x+\gamma_2(j-1)\Delta y)})\end{aligned}$$

$$= (1 - \tau W_1 - 4H_1 + H_2)\lambda^k e^{I(\gamma_1 i\Delta x + \gamma_2 j\Delta y)} + H_1\lambda^k (e^{I(\gamma_1 (i+1)\Delta x + \gamma_2 j\Delta y)} + e^{I(\gamma_1 (i-1)\Delta x + \gamma_2 j\Delta y)}) + H_1\lambda^k (e^{I(\gamma_1 i\Delta x + \gamma_2 (j+1)\Delta y)} + e^{I(\gamma_1 i\Delta x + \gamma_2 (j-1)\Delta y)}) + \tau \sum_{m=1}^{k-1} (W_{k-m} - W_{k-m+1})\,\lambda^m e^{I(\gamma_1 i\Delta x + \gamma_2 j\Delta y)} + \tau W_k \lambda^0 e^{I(\gamma_1 i\Delta x + \gamma_2 j\Delta y)}. \quad (23)$$

Upon simplification, we can get

$$\lambda^{k+1} = \frac{1 - \rho_1 - \rho_2 + H_2}{1 + \rho_1 + \rho_2 + H_2}\lambda^k + \frac{\tau}{1 + \rho_1 + \rho_2 + H_2}\left[\sum_{m=1}^{k-1} (W_{k-m} - W_{k-m+1})\,\lambda^m - W_1\lambda^k - W_k\lambda^0\right], \quad (24)$$

where

$$\rho_1 = 4H_1 \sin^2\left(\frac{\gamma_1 \Delta x}{2}\right),\ \rho_2 = 4H_1 \sin^2\left(\frac{\gamma_2 \Delta y}{2}\right).$$

We start with $k = 0$ in Eq. (27). Since $\rho_1,\ \rho_2 \geq 0$, then

$$|\lambda^1| = \left|\frac{1 - \rho_1 - \rho_2 + H_2}{1 + \rho_1 + \rho_2 + H_2}\right| |\lambda^0| \leq |\lambda^0|$$

Now, assume that $|\lambda^{s+1}| \leq |\lambda^0|$, $s = 0, 1, \ldots, k-1$. We need to prove this for $m = k$. Utilizing Eq. (27), we get

$$|\lambda^{k+1}| \leq \left|\frac{1 - \rho_1 - \rho_2 + H_2 - \tau W_1}{1 + \rho_1 + \rho_2 + H_2}\right| |\lambda^k| + \left|\frac{\tau}{1 + \rho_1 + \rho_2 + H_2}\right| \left[\sum_{m=1}^{k-1} |\,(W_{k-m} - W_{k-m+1})\,||\lambda^k| + |W_k||\lambda^0|\right].$$

Using induction hypothesis and lemma 1, we obtain

$$|\lambda^{k+1}| \leq \frac{|1 - \rho_1 - \rho_2 + H_2 - \tau W_1|}{1 + \rho_1 + \rho_2 + H_2}|\lambda^0| + \frac{\tau W_1}{1 + \rho_1 + \rho_2 + H_2}|\lambda^0|.$$

Consider the following two cases:
Case 1. If $1 - \rho_1 - \rho_2 + H_2 - \tau W_1 > 0$, then we have

$$|\lambda^{k+1}| \leq \frac{1 - \rho_1 - \rho_2 + H_2}{1 + \rho_1 + \rho_2 + H_2}|\lambda^0| \leq |\lambda^0|.$$

Case 2. $1 - \rho_1 - \rho_2 + H_2 - \tau W_1 < 0$, then we have

$$|\lambda^{k+1}| \leq \frac{-1 + \rho_1 + \rho_2 - H_2 + 2\tau W_1}{1 + \rho_1 + \rho_2 + H_2}|\lambda^0|.$$

Here,

$$|\lambda^{k+1}| \leq |\lambda^0| \Leftrightarrow -1 + \rho_1 + \rho_2 - H_2 + 2\tau W_1 \leq 1 + \rho_1 + \rho_2 + H_2 \Leftrightarrow 2 + 2H_2 - 2\tau W_1 \geq 0.$$

The proof is completed by mathematical induction. □

Theorem 1 *The C-N difference scheme* (10) *is stable if* $2 + 2H_2 - 2\tau W_1 \geq 0$.

Proof Utilizing lemma 2 and Parseval's equality, we obtain

$$\begin{aligned}\|\vartheta^k\|_2 &= \sum_{j=1}^{M_y-1}\sum_{i=1}^{M_x-1}\Delta y\Delta x|\vartheta_{i,j}^k|^2 = \Delta y\Delta x\sum_{j=1}^{M_y-1}\sum_{i=1}^{M_x-1}\left|\lambda^k e^{I(\gamma_1 i\Delta x+\gamma_2 j\Delta y)}\right|^2\\ &= \Delta y\Delta x\sum_{j=1}^{M_y-1}\sum_{i=1}^{M_x-1}|\lambda^k|^2 \le \Delta y\Delta x\sum_{j=1}^{M_y-1}\sum_{i=1}^{M_x-1}|\lambda^0|^2\\ &= \Delta y\Delta x\sum_{j=1}^{M_y-1}\sum_{i=1}^{M_x-1}\left|\lambda^0 e^{I(\gamma_1 i\Delta x+\gamma_2 j\Delta y)}\right|^2 = \|\vartheta^0\|_2.\end{aligned}$$

Thus, the difference scheme (10) is stable. □

Stability of the 2*h*-Spaced C-N Numerical Scheme

Let $\tilde{U}_{i,j}^k$ be the approximate solution of (14), and define

$$\zeta_{i,j}^k = U_{i,j}^k - \tilde{U}_{i,j}^k. \tag{25}$$

Substituting (25) into (14), we obtain

$$\begin{aligned}&(1+4G_1+G_2)\zeta_{i,j}^{k+1} - G_1(\zeta_{i+2,j}^{k+1}+\zeta_{i-2,j}^{k+1}) - G_1(\zeta_{i,j+2}^{k+1}+\zeta_{i,j-2}^{k+1})\\ &\quad= (1-\tau W_1-4G_1+G_2)\zeta_{i,j}^k + G_1(\zeta_{i+2,j}^k+\zeta_{i-2,j}^k) + G_1(\zeta_{i,j+2}^k+\zeta_{i,j-2}^k)\\ &\qquad+\tau\sum_{m=1}^{k-1}(W_{k-m}-W_{k-m+1})\,\zeta_{i,j}^m + \tau W_k\zeta_{i,j}^0.\end{aligned} \tag{26}$$

The Fourier series for $\zeta^k(x,y)$ is

$$\zeta^k(x,y) = \sum_{Z_1=-\infty}^{\infty}\sum_{Z_2=-\infty}^{\infty}\psi^k(Z_1,Z_2)e^{2\pi I(Z_1x/L+Z_2y/L)},$$

where $I=\sqrt{-1}$ and the Fourier coefficients $\psi^k(Z_1,Z_2)$ are given by

$$\psi^k(Z_1,Z_2) = \frac{1}{L^2}\int_0^L\int_0^L\zeta^k(x,y)e^{-2\pi I(Z_1x/L+Z_2y/L)}dxdy. \tag{27}$$

Introducing the following norm

$$\|\zeta^k\|_2 = \left(\sum_{j=1}^{M_y-1}\sum_{i=1}^{M_x-1}\Delta y\Delta x|\zeta_{i,j}^k|^2\right)^{1/2} = \left(\int_0^L\int_0^L|\zeta_{i,j}^k|^2dxdy\right)^{1/2}.$$

Applying the Parseval's equality

$$\int_0^L\int_0^L|\zeta_{i,j}^k|^2dxdy = \sum_{Z_2=-\infty}^{\infty}\sum_{Z_1=-\infty}^{\infty}|\psi^k(Z_1,Z_2)|^2,$$

we get

$$\|\zeta^k\|_2 = \left(\sum_{Z_2=-\infty}^{\infty}\sum_{Z_1=-\infty}^{\infty}|\psi^k(Z_1,Z_2)|^2\right)^{1/2}. \tag{28}$$

Based on the above analysis, we assume that the solution of Eq. (26) is of the following form

$$\zeta_{i,j}^{k} = \psi^{k} e^{I(\gamma_1 i\Delta x+\gamma_2 j\Delta y)}. \tag{29}$$

Lemma 3 *Suppose ψ^k is defined by (27). If $2 + 2G_2 - 2\tau W_1 \geq 0$, then we have*

$$|\psi^{k+1}| \leq |\psi^{0}|, \quad k = 0, 1, 2, \ldots, N-1.$$

Proof Substituting $\zeta_{i,j}^{k} = \psi^{k} e^{I(\gamma_1 i\Delta x+\gamma_2 j\Delta y)}$ into Eq. (26), we get

$$\begin{aligned}
&(1 + 4G_1 + G_2)\psi^{k+1} e^{I(\gamma_1 i\Delta x+\gamma_2 j\Delta y)} - G_1\psi^{k+1}(e^{I(\gamma_1 (i+2)\Delta x+\gamma_2 j\Delta y)} \\
&\quad + e^{I(\gamma_1 (i-2)\Delta x+\gamma_2 j\Delta y)}) - G_1\psi^{k+1}(e^{I(\gamma_1 i\Delta x+\gamma_2 (j+2)\Delta y)} + e^{I(\gamma_1 i\Delta x+\gamma_2 (j-2)\Delta y)}) \\
&= (1 - \tau W_1 - 4G_1 + G_2)\psi^{k} e^{I(\gamma_1 i\Delta x+\gamma_2 j\Delta y)} + G_1\psi^{k}(e^{I(\gamma_1 (i+2)\Delta x+\gamma_2 j\Delta y)} \\
&\quad + e^{I(\gamma_1 (i-2)\Delta x+\gamma_2 j\Delta y)}) + G_1\psi^{k}(e^{I(\gamma_1 i\Delta x+\gamma_2 (j+2)\Delta y)} + e^{I(\gamma_1 i\Delta x+\gamma_2 (j-2)\Delta y)}) \\
&\quad + \tau\sum_{m=1}^{k-1}(W_{k-m} - W_{k-m+1})\,\psi^{m} e^{I(\gamma_1 i\Delta x+\gamma_2 j\Delta y)} + \tau W_k \psi^{0} e^{I(\gamma_1 i\Delta x+\gamma_2 j\Delta y)}.
\end{aligned} \tag{30}$$

After simplification, we can get

$$\begin{aligned}
\psi^{k+1} =& \frac{1 - \kappa_1 - \kappa_2 + G_2}{1 + \kappa_1 + \kappa_2 + G_2}\psi^{k} \\
&+ \frac{\tau}{1 + \kappa_1 + \kappa_2 + G_2}\left[\sum_{m=1}^{k-1}(W_{k-m} - W_{k-m+1})\,\psi^{m} - W_1\psi^{k} - W_k\psi^{0}\right],
\end{aligned} \tag{31}$$

where

$$\kappa_1 = 4G_1\sin^2(\gamma_1\Delta x),\ \kappa_2 = 4G_1\sin^2(\gamma_2\Delta y).$$

Letting $k = 0$ in Eq. (31) and using that $\kappa_1,\ \kappa_2 \geq 0$, we obtain

$$|\psi^{1}| = \left|\frac{1 - \kappa_1 - \kappa_2 + G_2}{1 + \kappa_1 + \kappa_2 + G_2}\right||\psi^{0}| \leq |\psi^{0}|$$

Now, suppose that $|\psi^{s+1}| \leq |\psi^{0}|$, $s = 0, 1, \ldots, k-1$. We must prove it holds for $m = k$. Using Eq. (31), we get

$$\begin{aligned}
|\psi^{k+1}| \leq& \left|\frac{1 - \kappa_1 - \kappa_2 + G_2 - \tau W_1}{1 + \kappa_1 + \kappa_2 + G_2}\right||\psi^{k}| \\
&+ \left|\frac{\tau}{1 + \kappa_1 + \kappa_2 + G_2}\right|\left[\sum_{m=1}^{k-1}|\,(W_{k-m} - W_{k-m+1})\,||\psi^{k}| + |W_k||\psi^{0}|\right].
\end{aligned}$$

By the induction hypothesis and lemma 1, we get

$$|\psi^{k+1}| \leq \frac{|1 - \kappa_1 - \kappa_2 + G_2 - \tau W_1| + \tau W_1}{1 + \kappa_1 + \kappa_2 + G_2}|\psi^{0}|.$$

Consider the following two cases:
Case 1. If $1 - \kappa_1 - \kappa_2 + G_2 - \tau W_1 > 0$, then we have

$$|\psi^{k+1}| \leq \frac{1 - \kappa_1 - \kappa_2 + G_2}{1 + \kappa_1 + \kappa_2 + G_2}|\psi^{0}| \leq |\psi^{0}|.$$

Case 2. $1-\kappa_1-\kappa_2+G_2-\tau W_1<0$, then we have

$$|\psi^{k+1}| \le \frac{-1+\kappa_1+\kappa_2-G_2+2\tau W_1}{1+\kappa_1+\kappa_2+G_2}|\psi^0|.$$

Here,

$$\begin{aligned}|\psi^{k+1}| &\le |\psi^0| \\ &\Leftrightarrow -1+\kappa_1+\kappa_2-G_2+2\tau W_1 \le 1+\kappa_1+\kappa_2+G_2 \\ &\Leftrightarrow 2+2G_2-2\tau W_1 \ge 0.\end{aligned}$$

This completes the proof. □

Theorem 2 *The C-N difference scheme* (14) *is stable if* $2+2G_2-2\tau W_1 \ge 0$.

Proof Utilizing lemma 3 and Parseval's equality, we obtain

$$\begin{aligned}\|\zeta^k\|_2 &= \sum_{j=1}^{M_y-1}\sum_{i=1}^{M_x-1}\Delta y\Delta x|\zeta_{i,j}^k|^2 = \Delta y\Delta x\sum_{j=1}^{M_y-1}\sum_{i=1}^{M_x-1}\left|\psi^k e^{I(\gamma_1 i\Delta x+\gamma_2 j\Delta y)}\right|^2 \\ &= \Delta y\Delta x\sum_{j=1}^{M_y-1}\sum_{i=1}^{M_x-1}|\psi^k|^2 \le \Delta y\Delta x\sum_{j=1}^{M_y-1}\sum_{i=1}^{M_x-1}|\psi^0|^2 \\ &= \Delta y\Delta x\sum_{j=1}^{M_y-1}\sum_{i=1}^{M_x-1}\left|\psi^0 e^{I(\gamma_1 i\Delta x+\gamma_2 j\Delta y)}\right|^2 = \|\zeta^0\|_2,\end{aligned}$$

which means that the difference scheme (14) is stable. □

Convergence Analysis

In this section, the convergence of the proposed methods is investigated. By subtracting Eq. (10) from Eq. (9) and defining $\varepsilon_{i,j}^k = u(x_i,y_j,t_k)-U_{i,j}^k$, the following error equation is obtained

$$\begin{aligned}&(1+4H_1+H_2)\varepsilon_{i,j}^{k+1}-H_1(\varepsilon_{i+1,j}^{k+1}+\varepsilon_{i-1,j}^{k+1})-H_1(\varepsilon_{i,j+1}^{k+1}+\varepsilon_{i,j-1}^{k+1}) \\ &\quad=(1-\tau W_1-4H_1+H_2)\varepsilon_{i,j}^k+H_1(\varepsilon_{i+1,j}^k+\varepsilon_{i-1,j}^k)+H_1(\varepsilon_{i,j+1}^k+\varepsilon_{i,j-1}^k) \\ &\qquad+\tau\sum_{m=1}^{k-1}(W_{k-m}-W_{k-m+1})\,\varepsilon_{i,j}^m+\tau W_k\varepsilon_{i,j}^0+\tau R_{i,j}^{k+1/2}.\end{aligned} \tag{32}$$

From Eq. (9), there is a positive constant C_1 such that

$$|R_{i,j}^{k+1/2}| \le C_1(\tau^{2-\alpha}+h^2). \tag{33}$$

Similar to the stability analysis, $\varepsilon^k(x,y)$ and $R^{k+1/2}(x,y)$ can be expanded in Fourier series as

$$\varepsilon^k(x,y) = \sum_{Z_2=-\infty}^{\infty}\sum_{Z_1=-\infty}^{\infty}\eta^k(Z_1,Z_2)e^{2\pi I(Z_1x/L+Z_2y/L)},$$

$$R^{k+1/2}(x,y)=\sum_{Z_2=-\infty}^{\infty}\sum_{Z_1=-\infty}^{\infty}\varphi^k(Z_1,Z_2)e^{2\pi I(Z_1x/L+Z_2y/L)},$$

where the Fourier coefficients η^k and φ^k are

$$\eta^k(Z_1,Z_2)=\frac{1}{L^2}\int_0^L\int_0^L\varepsilon^k(x,y)e^{-2\pi I(Z_1x/L+Z_2y/L)}dxdy,$$
$$\varphi^k(Z_1,Z_2)=\frac{1}{L^2}\int_0^L\int_0^L R^{k+1/2}(x,y)e^{-2\pi I(Z_1x/L+Z_2y/L)}dxdy.$$

By making use of the Parseval's equality and L^2 norm, we obtain

$$\begin{aligned}\|\varepsilon^k\|_2&=\left(\sum_{j=1}^{M_y-1}\sum_{i=1}^{M_x-1}\Delta y\Delta x|\varepsilon_{i,j}^k|^2\right)^{1/2}\\&=\left(\sum_{Z_1=-\infty}^{\infty}\sum_{Z_2=-\infty}^{\infty}|\eta^k(Z_1,Z_2)|^2\right)^{1/2},\end{aligned}\tag{34}$$

$$\begin{aligned}\|R^{k+1/2}\|_2&=\left(\sum_{j=1}^{M_y-1}\sum_{i=1}^{M_x-1}\Delta y\Delta x|R_{i,j}^{k+1/2}|^2\right)^{1/2}\\&=\left(\sum_{Z_1=-\infty}^{\infty}\sum_{Z_2=-\infty}^{\infty}|\varphi^k(Z_1,Z_2)|^2\right)^{1/2}.\end{aligned}\tag{35}$$

Next, we suppose the solutions of Eq. (32) are as follows

$$\varepsilon_{i,j}^k=\eta^k e^{I(\gamma_1 i\Delta x+\gamma_2 j\Delta y)},\ R_{i,j}^{k+1/2}=\varphi^k e^{I(\gamma_1 i\Delta x+\gamma_2 j\Delta y)}.\tag{36}$$

Using the assumptions in (36) and considering (32), we obtain

$$\begin{aligned}&(1+4H_1+H_2)\eta^{k+1}e^{I(\gamma_1 i\Delta x+\gamma_2 j\Delta y)}-H_1\eta^{k+1}(e^{I(\gamma_1(i+1)\Delta x+\gamma_2 j\Delta y)}\\&\quad+e^{I(\gamma_1(i-1)\Delta x+\gamma_2 j\Delta y)})-H_1\eta^{k+1}(e^{I(\gamma_1 i\Delta x+\gamma_2(j+1)\Delta y)}+e^{I(\gamma_1 i\Delta x+\gamma_2(j-1)\Delta y)})\\&=(1-\tau W_1-4H_1+H_2)\eta^k e^{I(\gamma_1 i\Delta x+\gamma_2 j\Delta y)}+H_1\eta^k(e^{I(\gamma_1(i+1)\Delta x+\gamma_2 j\Delta y)}\\&\quad+e^{I(\gamma_1(i-1)\Delta x+\gamma_2 j\Delta y)})+H_1\eta^k(e^{I(\gamma_1 i\Delta x+\gamma_2(j+1)\Delta y)}+e^{I(\gamma_1 i\Delta x+\gamma_2(j-1)\Delta y)})\\&\quad+\tau\sum_{m=1}^{k-1}(W_{k-m}-W_{k-m+1})\,\eta^m e^{I(\gamma_1 i\Delta x+\gamma_2 j\Delta y)}+\tau W_k\eta^0 e^{I(\gamma_1 i\Delta x+\gamma_2 j\Delta y)}\\&\quad+\tau\varphi^{k+1/2}e^{I(\gamma_1 i\Delta x+\gamma_2 j\Delta y)}.\end{aligned}\tag{37}$$

After simplification, we have

$$\begin{aligned}\eta^{k+1}&=\frac{1-\rho_1-\rho_2+H_2}{1+\rho_1+\rho_2+H_2}\eta^k\\&\quad+\frac{\tau}{1+\rho_1+\rho_2+H_2}\left[\sum_{m=1}^{k-1}(W_{k-m}-W_{k-m+1})\,\eta^m-W_1\eta^k+\varphi^{k+1/2}\right],\end{aligned}\tag{38}$$

where ρ_1 and ρ_2 are as defined in the previous section.

Due to the convergence of the series in the right hand side of Eq. (35), there is a positive constant C_2 such that

$$|\varphi^{k+1/2}| = |\varphi^{k+1/2}(Z_1, Z_2)| \le C_2|\varphi^{1/2}(Z_1, Z_2)| = C_2|\varphi^{1/2}|. \tag{39}$$

Lemma 4 *Suppose η^{k+1} and $\varphi^{k+1/2}$ satisfy Eq. (38). If $2 + 2H_2 - \tau(2W_1 - W_k) \ge 0$, then we have*

$$|\eta^{k+1}| \le C_2(k+1)\tau|\varphi^{1/2}|, \quad k = 0, 1, \ldots, N-1.$$

Proof Noticing that $\eta^0 = \eta^0(Z_1, Z_2) = 0$. Then, for $k = 0$, we have

$$|\eta^1| = \left|\frac{1}{1+\rho_1+\rho_2+H_2}\right||\tau\varphi^{1/2}| \le \tau|\varphi^{1/2}| \le C_2\tau|\varphi^{1/2}|.$$

Now, assume that $|\eta^{s+1}| \le C_2(s+1)\tau|\varphi^{1/2}|$, $s = 0, 1, \ldots, k-1$. We need to prove this for $s = k$. From Eq. (38), we have

$$\begin{aligned}|\eta^{k+1}| \le & \left|\frac{1-\rho_1-\rho_2+H_2-\tau W_1}{1+\rho_1+\rho_2+H_2}\right||\eta^k| \\ & + \left|\frac{\tau}{1+\rho_1+\rho_2+H_2}\right|\left[\sum_{m=1}^{k-1}|(W_{k-m} - W_{k-m+1})||\eta^k| + |\varphi^{k+1/2}|\right].\end{aligned}$$

Utilizing induction hypothesis, lemma 1 and Eq. (39), we get

$$|\eta^{k+1}| \le \left[\frac{|1-\rho_1-\rho_2+H_2-\tau W_1| + \tau(W_1 - W_k)}{1+\rho_1+\rho_2+H_2}k + \frac{1}{1+\rho_1+\rho_2+H_2}\right]C_2\tau|\varphi^{1/2}|.$$

If $1 - \rho_1 - \rho_2 + H_2 - \tau W_1 > 0$, then we have

$$\begin{aligned}|\eta^{k+1}| &\le \left[\frac{1-\rho_1-\rho_2+H_2-\tau W_k}{1+\rho_1+\rho_2+H_2}k + \frac{1}{1+\rho_1+\rho_2+H_2}\right]C_2\tau|\varphi^{1/2}| \\ &\le C_2(k+1)\tau|\varphi^{1/2}|.\end{aligned}$$

If $1 - \rho_1 - \rho_2 + H_2 - \tau W_1 < 0$, then we have

$$|\eta^{k+1}| \le \left[\frac{-1+\rho_1+\rho_2-H_2+\tau(2W_1 - W_k)}{1+\rho_1+\rho_2+H_2}k + \frac{1}{1+\rho_1+\rho_2+H_2}\right]C_2\tau|\varphi^{1/2}|.$$

Here,

$$\begin{aligned}&|\eta^{k+1}| \le C_2(k+1)\tau|\varphi^{1/2}| \\ &\quad \Leftrightarrow -1+\rho_1+\rho_2-H_2+\tau(2W_1-W_k) \le 1+\rho_1+\rho_2+H_2 \\ &\quad \Leftrightarrow 2+2H_2-\tau(2W_1-W_k) \ge 0.\end{aligned}$$

This completes the proof. □

Theorem 3 *The C-N difference scheme (10) is convergent and the order of convergence is $O(\tau^{2-\alpha} + h^2)$.*

Proof Using lemma 4 and Parseval's equality, we obtain

$$\|\varepsilon^k\|_2^2 = \sum_{j=1}^{M_y-1}\sum_{i=1}^{M_x-1} \Delta y\Delta x|\varepsilon_{i,j}^k|^2 = \Delta y\Delta x \sum_{j=1}^{M_y-1}\sum_{i=1}^{M_x-1} \left|\eta^k e^{I(\gamma_1 i\Delta x+\gamma_2 j\Delta y)}\right|^2$$
$$= \Delta y\Delta x \sum_{j=1}^{M_y-1}\sum_{i=1}^{M_x-1} |\eta^k|^2 \le C_2^2(k+1)^2\tau^2\Delta y\Delta x \sum_{j=1}^{M_y-1}\sum_{i=1}^{M_x-1} |\varphi^{1/2}|^2$$
$$= C_2^2(k+1)^2\tau^2\Delta y\Delta x \sum_{j=1}^{M_y-1}\sum_{i=1}^{M_x-1} \left|\varphi^{1/2} e^{I(\gamma_1 i\Delta x+\gamma_2 j\Delta y)}\right|^2 = C_2^2(k+1)^2\tau^2\|R^{1/2}\|_2^2.$$

Noticing that $(k+1)\tau \le T$ and letting $C = C_1C_2T$. From Eq. (33), we have

$$\|\varepsilon^k\|_2 \le C(\tau^{2-\alpha} + h^2),$$

which completes the proof. □

Theorem 4 *The C-N difference scheme* (14) *is convergent and the order of convergence is* $O(\tau^{2-\alpha} + h^2)$.

Proof The proof is similar to Theorem 3. □

Numerical Experiments

In this part, three test problems with known exact solutions are simulated on Windows 10 (64 bit) Intel (R) Core (TM) i7-8550U CPU 2.00 GHz, 8GB of RAM utilizing MATLAB software. The numerical results are obtained at three different final times, namely, $T = 4$, $T = 8$ and $T = 12$ with the spatial domain being restricted to $\Omega = (0, 1)^2$. The proposed methods are combined with the Gauss-Seidel iterative scheme with error tolerance of 10^{-5} to solve the test problems of the form in Eq. (1). Throughout the discussion, we let u, U_{C-N}, U_{FEG} and U_{MFEG} denote the exact, C-N, FEG and MFEG solutions, respectively. In addition, the computational orders of the presented methods are calculated using the formula [47]

$$\text{C-Order} = \frac{log(E_\infty(\tau, h_1)/E_\infty(\tau, h_2))}{log(h_1/h_2)}$$

Test Problem 6.1 In the first problem, consider the source term as follows

$$f(x, y, t) = \left(2t + \frac{2}{\Gamma(3-\alpha)}t^{2-\alpha} + 2t^2\pi^2\right)\cos(\pi x)\cos(\pi y),$$

where the exact solution is given by

$$u(x, y, t) = t^2\cos(\pi x)\cos(\pi y).$$

Tables 1, 2 and 3 show the numerical results of the elapsed time (in seconds), number of iterations (Ite) and maximum absolute error ($E_\infty(\tau, h)$) for the C-N, FEG and MFEG schemes with $T = 4$, $N = 100$, α=0.1, 0.3, 0.7 for different sizes of space steps, respectively. Figure 3 presents a comparison of the exact solution and other numerical solutions obtained at $\alpha = 0.3$, $N = 100$, $h^{-1} = 42$ and $y = 0.119$. In addition, the graphical error representation of the C-N scheme for $T = 4$, $\alpha = 0.3$, $N = 100$ and $h^{-1} = 42$ is depicted in Fig. 4 while

Table 1 Comparison between C-N, FEG and MFEG methods for Test Problem 6.1 with $\alpha = 0.1$, $T = 4$ and $N = 100$

h^{-1}	C-N			FEG			MFEG		
	Time	Ite	$E_\infty(\tau, h)$	Time	Ite	$E_\infty(\tau, h)$	Time	Ite	$E_\infty(\tau, h)$
10	0.4175	23	2.2757E-02	0.3356	15	2.2754E-02	0.0945	6	8.6466E-02
18	2.3110	52	6.9678E-03	1.0515	31	6.9591E-03	0.2451	12	2.7489E-02
26	5.8888	92	3.3755E-03	4.1425	53	3.3677E-03	0.4943	19	1.3548E-02
34	18.2440	140	1.9430E-03	10.1393	80	1.9427E-03	1.1403	28	7.9289E-03
42	39.2082	196	1.2113E-03	20.9560	111	1.2394E-03	2.6987	37	5.1846E-03

Table 2 Comparison between C-N, FEG and MFEG methods for Test Problem 6.1 with $\alpha = 0.3$, $T = 4$ and $N = 100$

h^{-1}	C-N			FEG			MFEG		
	Time	Ite	$E_\infty(\tau, h)$	Time	Ite	$E_\infty(\tau, h)$	Time	Ite	$E_\infty(\tau, h)$
10	0.3476	22	2.2785E-02	0.2483	15	2.2778E-02	0.0920	6	8.6576E-02
18	1.6289	51	6.9747E-03	1.0755	31	6.9638E-03	0.2450	12	2.7522E-02
26	6.5401	90	3.3776E-03	3.8171	52	3.3693E-03	0.6294	19	1.3561E-02
34	18.1564	138	1.9419E-03	9.9377	79	1.9423E-03	1.2881	27	7.9373E-03
42	39.9924	194	1.2115E-03	21.2502	110	1.2385E-03	2.1786	37	5.1877E-03

Table 3 Comparison between C-N, FEG and MFEG methods for Test Problem 6.1 with $\alpha = 0.7$, $T = 4$ and $N = 100$

h^{-1}	C-N			FEG			MFEG		
	Time	Ite	$E_\infty(\tau, h)$	Time	Ite	$E_\infty(\tau, h)$	Time	Ite	$E_\infty(\tau, h)$
10	0.4374	20	2.2831E-02	0.3357	18	2.2823E-02	0.1252	6	8.6801E-02
18	1.5666	47	6.9786E-03	0.924	28	6.9697E-03	0.2853	11	2.7583E-02
26	4.4705	83	3.3703E-03	2.9016	48	3.3642E-03	0.5462	17	1.3582E-02
34	11.6037	126	1.9280E-03	6.6387	72	1.9324E-03	1.1091	25	7.9436E-03
42	28.1122	177	1.1913E-03	13.7709	101	1.2262E-03	1.7506	34	5.1873E-03

its second order convergence can be observed from the results in Table 4. From the data in these tables and figures, the convergence of the presented methods is confirmed. Comparing the resolution of the tested methods, it may be observed that the C-N and FEG schemes have almost the same degree of accuracy while the magnitude of absolute errors for the MFEG method is slightly larger than the said schemes. This is because the iterative process for the C-N and FEG schemes is implemented on a mesh size of h while the iterative process of the MFEG method is carried out on a mesh size of $2h$; hence, increasing the error term by 4. Figure 5 compares the computing times and iteration numbers of the tested methods and shows that the FEG and MFEG methods are more efficient than the C-N difference scheme in terms of execution time and number of iterations.

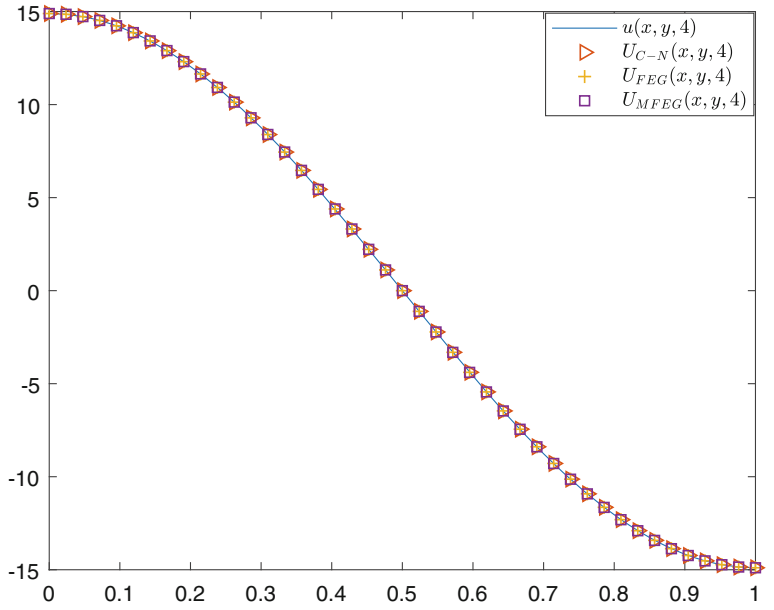

Fig. 3 Comparison of exact and numerical solutions for Test Problem 6.1 with $\alpha = 0.3$, $T = 4$, $h^{-1} = 42$, $N = 100$ and $y = 0.119$

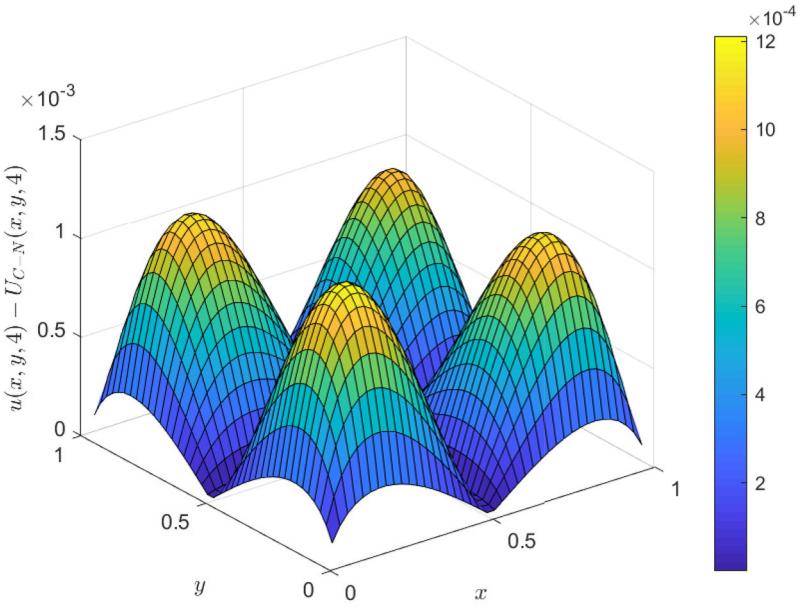

Fig. 4 Surface error plot of the C-N method for Test Problem 6.1 with $\alpha = 0.3$, $T = 4$, $h^{-1} = 42$ and $N = 100$

Table 4 Maximum errors and computational orders of the C-N method for Test problem 6.1 with $T = 1$ and $\tau = 0.001$

$\alpha = 0.1$			$\alpha = 0.5$			$\alpha = 0.9$		
h^{-1}	$E_\infty(\tau, h)$	C-Order	h^{-1}	$E_\infty(\tau, h)$	C-Order	h^{-1}	$E_\infty(\tau, h)$	C-Order
6	3.6027E-03	–	6	3.5845E-03	–	6	3.5656E-03	–
10	1.3960E-03	1.8560	10	1.3888E-03	1.8562	10	1.3818E-03	1.8557
14	7.1168E-04	2.0024	14	7.0804E-04	2.0022	14	7.0537E-04	1.9984
18	4.2523E-04	2.0492	18	4.2318E-04	2.0480	18	4.1537E-04	2.1071

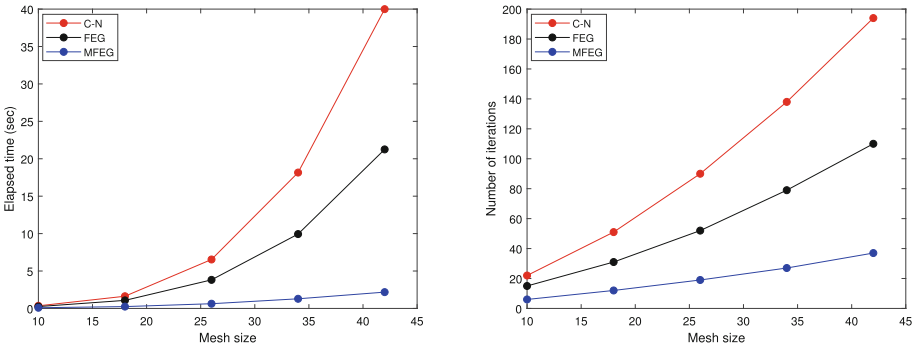

(a) Elapsed time (b) Number of iterations

Fig. 5 The graphs of (a) elapsed time and (b) number of iterations of the proposed methods for Test Problem 6.1 with $\alpha = 0.3$

Test Problem 6.2 In the second problem, we consider the source term given by

$$f(x, y, t) = \big((1+\alpha)t^\alpha + \Gamma(2+\alpha)t - 4t^{1+\alpha}(x-0.5)^2 - 4t^{1+\alpha}(y-0.5)^2 + 4t^{1+\alpha}\big)e^{-(x-0.5)^2-(y-0.5)^2},$$

and the corresponding exact solution

$$u(x, y, t) = e^{-(x-0.5)^2-(y-0.5)^2}t^{1+\alpha}.$$

The initial and boundary conditions are extracted from the exact solution. The exact, C-N, FEG and MFEG solutions at $\alpha = 0.5$, $N = 100$, $h^{-1} = 42$ and $y = 0.5$ are portrayed in Fig. 6, while Fig. 7 demonstrates the surface of absolute errors of the FEG method for $T = 8$ and $\alpha = 0.5$, $N = 100$ and $h^{-1} = 42$. From the figures, it can be observed that the numerical solutions match well with the exact solution. Tables 5, 6 and 7 display the numerical results of the proposed methods with $T = 8$, $N = 100$ and α=0.3, 0.5, 0.7 for various space steps, respectively. Furthermore, Fig. 8 illustrates the computational times and number of iterations pertained to the three tested methods. The elapsed time and iterations number in Tables 5, 6 and 7 and Fig. 8 indicate that the computational cost of the fractional group methods (FEG and MFEG) is lower than the C-N scheme, which show the effectiveness of the former. Table 8 show the numerical errors and computational orders computed using the FEG method. Just as we expect, the second order convergence can be seen from the data recorded in this table.

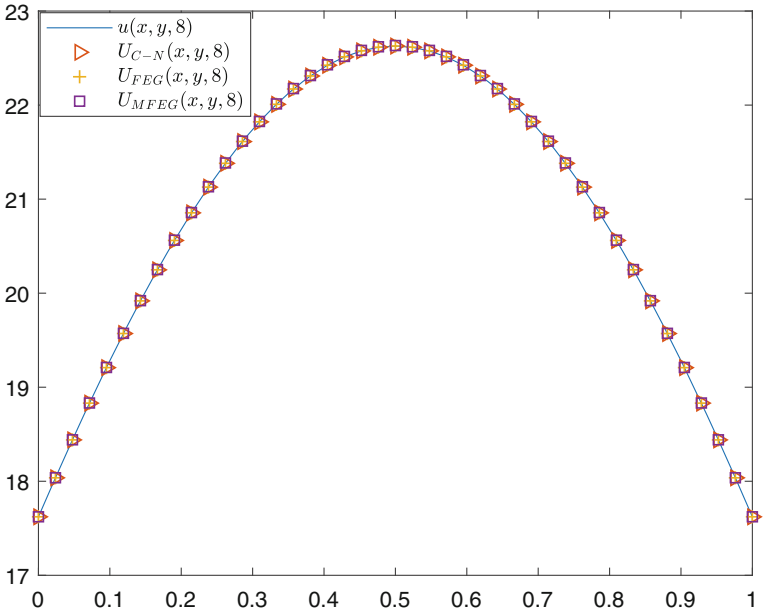

Fig. 6 Comparison of exact and numerical solutions for Test Problem 6.2 with $\alpha = 0.5$, $T = 8$, $h^{-1} = 42$, $N = 100$ and $y = 0.5$

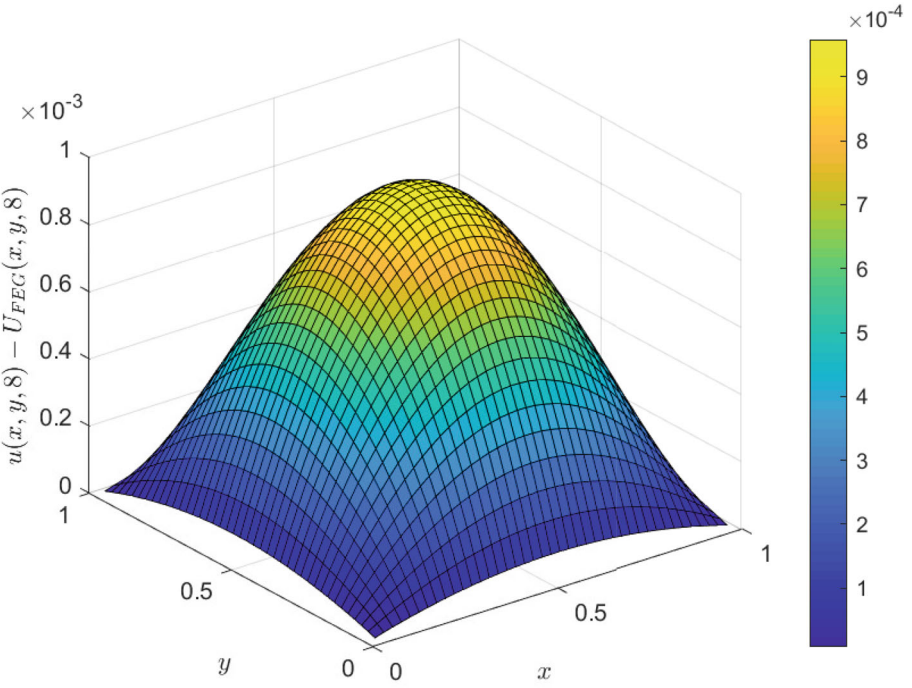

Fig. 7 Surface error plot of the FEG method for Test Problem 6.2 with $\alpha = 0.5$, $T = 8$, $h^{-1} = 42$ and $N = 100$

Table 5 Comparison between C-N, FEG and MFEG methods for Test Problem 6.2 with $\alpha = 0.3$, $T = 8$ and $N = 100$

h^{-1}	C-N			FEG			MFEG		
	Time	Ite	$E_\infty(\tau, h)$	Time	Ite	$E_\infty(\tau, h)$	Time	Ite	$E_\infty(\tau, h)$
10	0.8609	40	1.6822E-02	0.3782	24	1.6841E-02	0.1286	9	6.4272E-02
18	3.7968	107	5.0513E-03	2.6769	60	5.1250E-03	0.3748	19	2.0512E-02
26	14.3701	199	2.1594E-03	8.6991	111	2.3224E-03	1.2356	35	9.8791E-03
34	42.6815	312	8.8053E-04	22.9559	175	1.1698E-03	2.0979	54	5.7423E-03
42	57.6235	444	1.2502E-04	43.8745	249	5.0909E-04	4.3400	77	3.7024E-03

Table 6 Comparison between C-N, FEG and MFEG methods for Test Problem 6.2 with $\alpha = 0.5$, $T = 8$ and $N = 100$

h^{-1}	C-N			FEG			MFEG		
	Time	Ite	$E_\infty(\tau, h)$	Time	Ite	$E_\infty(\tau, h)$	Time	Ite	$E_\infty(\tau, h)$
10	0.6385	40	2.5633E-02	0.3369	24	2.5655E-02	0.1324	9	9.8056E-02
18	3.9289	109	7.7312E-03	2.6144	61	7.8090E-03	0.3197	20	3.1264E-02
26	15.1236	205	3.4143E-03	8.4977	114	3.5836E-03	1.1475	35	1.5038E-02
34	43.1109	324	1.5899E-03	22.6807	180	1.8797E-03	2.6300	55	8.7478E-03
42	57.5005	463	5.2261E-04	45.1226	258	9.5837E-04	4.0916	79	5.6592E-03

Table 7 Comparison between C-N, FEG and MFEG methods for Test Problem 6.2 with $\alpha = 0.7$, $T = 8$ and $N = 100$

h^{-1}	C-N			FEG			MFEG		
	Time	Ite	$E_\infty(\tau, h)$	Time	Ite	$E_\infty(\tau, h)$	Time	Ite	$E_\infty(\tau, h)$
10	0.7414	39	3.8935E-02	0.4136	24	3.8961E-02	0.1449	9	1.4920E-01
18	2.8969	107	1.1739E-02	1.9721	60	1.1820E-02	0.3785	19	4.7492E-02
26	10.8329	202	5.2526E-03	6.222	112	5.4286E-03	0.8366	35	2.2808E-02
34	35.868	322	2.6066E-03	16.4327	177	2.8908E-03	1.6588	54	1.3244E-02
42	69.2403	462	1.1268E-03	39.3033	255	1.5682E-03	3.3176	77	8.5538E-03

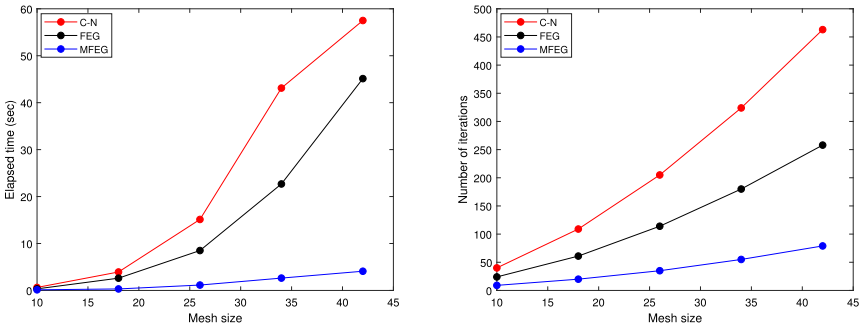

(a) Elapsed time (b) Number of iterations

Fig. 8 The graphs of (a) elapsed time and (b) number of iterations of the proposed methods for Test Problem 6.2 with $\alpha = 0.5$

Table 8 Maximum errors and computational orders of the FEG method for Test problem 6.2 with $T = 1$ and $\tau = 0.001$

$\alpha = 0.1$			$\alpha = 0.5$			$\alpha = 0.9$		
h^{-1}	$E_\infty(\tau, h)$	C-Order	h^{-1}	$E_\infty(\tau, h)$	C-Order	h^{-1}	$E_\infty(\tau, h)$	C-Order
6	2.9156E-03	–	6	2.8109E-03	–	6	2.6749E-03	–
10	1.0516E-03	1.9963	10	1.0135E-03	1.997	10	9.6529E-04	1.9953
14	5.3744E-04	1.995	14	5.1799E-04	1.9948	14	4.9175E-04	2.0045
18	3.1750E-04	2.0943	18	3.0390E-04	2.1219	18	2.9426E-04	2.0433

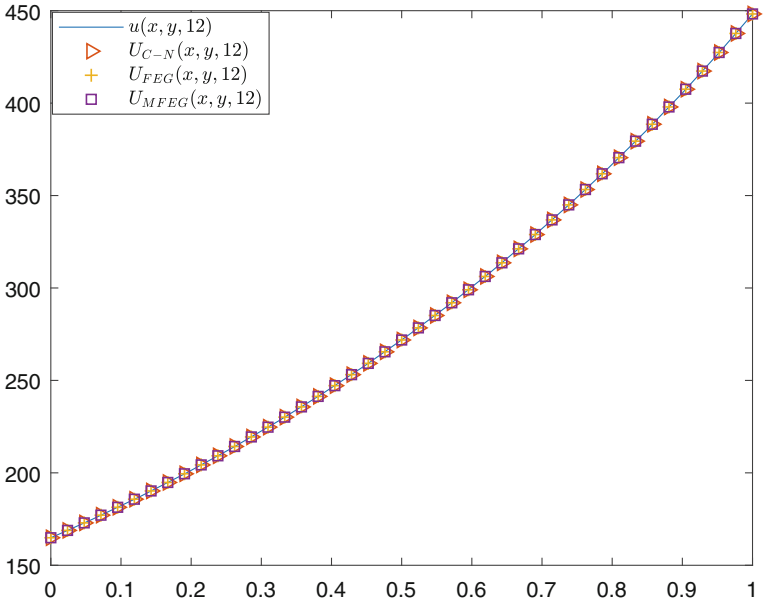

Fig. 9 Comparison of exact and numerical solutions for Test Problem 6.3 with $\alpha = 0.7$, $T = 12$, $h^{-1} = 42$, $N = 100$ and $y = 0.881$

Test Problem 6.3 In this problem, the following source term is considered

$$f(x, y, t) = \left((1+\alpha)t^{\alpha} + \Gamma(2+\alpha)t - 2t^{1+\alpha}\right) e^{x+y},$$

along with the exact solution

$$u(x, y, t) = t^{1+\alpha} e^{x+y}.$$

Again, the initial and boundary conditions can be drawn from the exact solution. In Fig. 9, we sketch the exact solution together with the numerical solutions obtained at $\alpha = 0.7$, $N = 100$, $h^{-1} = 42$ and $y = 0.881$, while in Fig. 10 we draw the surface figure of maximum absolute errors of the MFEG method for $T = 12$, $\alpha = 0.7$, $N = 100$ and $h^{-1} = 42$. The figures illustrate the accuracy of the proposed methods. In Tables 9, 10 and 11, experimental results of the C-N, FEG and MFEG methods with $T = 12$, $N = 100$ and α= 0.3, 0.5, 0.7 for various mesh sizes are recorded, respectively. Both of the elapsed time and the number of iterations versus different mesh sizes are depicted in Fig. 11. Similar to the previous tests, it

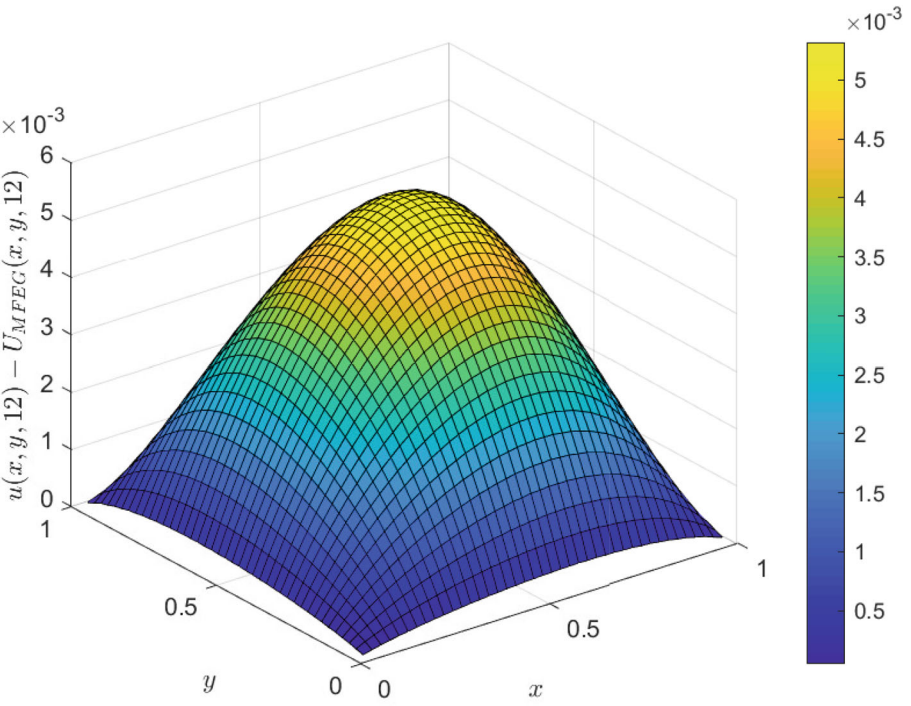

Fig. 10 Surface error plot of the FEG method for Test Problem 6.3 with $\alpha = 0.7$, $T = 12$, $h^{-1} = 42$ and $N = 100$

Table 9 Comparison between C-N, FEG and MFEG methods for Test Problem 6.3 with $\alpha = 0.3$, $T = 12$ and $N = 100$

h^{-1}	C-N			FEG			MFEG		
	Time	Ite	$E_\infty(\tau, h)$	Time	Ite	$E_\infty(\tau, h)$	Time	Ite	$E_\infty(\tau, h)$
10	0.9338	56	8.6771E-03	0.4457	33	8.6925E-03	0.1402	11	3.3764E-02
18	3.9919	155	2.5894E-03	2.5803	86	2.6599E-03	0.3867	26	1.0715E-02
26	16.5821	295	1.0450E-03	9.1018	162	1.1852E-03	1.1168	49	5.1784E-03
34	32.0802	471	3.6668E-04	25.2729	258	5.5033E-04	2.4359	77	3.0052E-03
42	64.4505	678	3.8897E-04	55.5592	373	2.1681E-04	4.7049	111	1.9285E-03

Table 10 Comparison between C-N, FEG and MFEG methods for Test Problem 6.3 with $\alpha = 0.5$, $T = 12$ and $N = 100$

h^{-1}	C-N			FEG			MFEG		
	Time	Ite	$E_\infty(\tau, h)$	Time	Ite	$E_\infty(\tau, h)$	Time	Ite	$E_\infty(\tau, h)$
10	0.7929	57	1.4381E-02	0.4910	33	1.4393E-02	0.1278	11	5.5926E-02
18	4.2983	159	4.3691E-03	2.5652	88	4.4432E-03	0.3977	27	1.7753E-02
26	16.7838	304	1.8992E-03	9.7074	166	2.0478E-03	1.1253	49	8.5798E-03
34	34.1840	487	8.2457E-04	25.7286	265	1.0484E-03	2.4011	78	4.9996E-03
42	78.4912	704	2.7888E-04	56.3769	384	5.0444E-04	4.4506	113	3.2386E-03

Table 11 Comparison between C-N, FEG and MFEG methods for Test Problem 6.3 with $\alpha = 0.7$, $T = 12$ and $N = 100$

h^{-1}	C-N			FEG			MFEG		
	Time	Ite	$E_\infty(\tau, h)$	Time	Ite	$E_\infty(\tau, h)$	Time	Ite	$E_\infty(\tau, h)$
10	0.7322	56	2.3677E-02	0.4408	33	2.3693E-02	0.1277	11	9.2293E-02
18	4.1288	157	7.2080E-03	2.5156	87	7.2878E-03	0.3377	26	2.9239E-02
26	16.0169	302	3.2214E-03	8.8714	164	3.3752E-03	1.1323	49	1.4102E-02
34	35.1462	487	1.5531E-03	25.0797	264	1.7958E-03	2.3041	77	8.2001E-03
42	77.8330	707	6.4924E-04	55.6289	383	9.5072E-04	4.4194	112	5.3181E-03

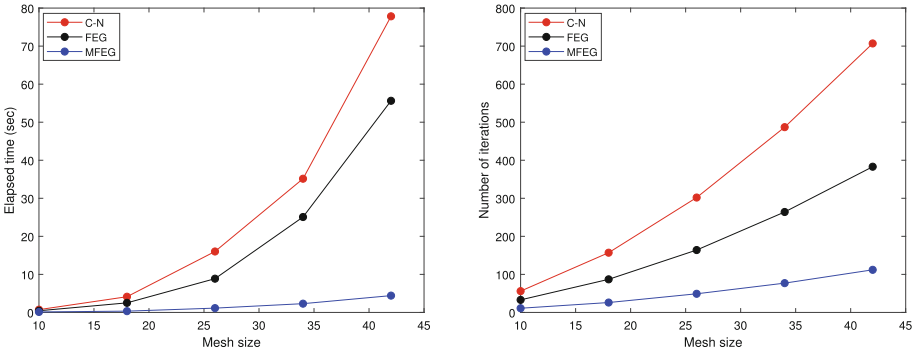

(a) Elapsed time (b) Number of iterations

Fig. 11 The graphs of (a) elapsed time and (b) number of iterations of the proposed methods for Test Problem 6.3 with $\alpha = 0.7$

Table 12 Maximum errors and computational orders of the MFEG method for Test problem 6.3 with $T = 1$ and $\tau = 0.001$

$\alpha = 0.1$			$\alpha = 0.5$			$\alpha = 0.9$		
h^{-1}	$E_\infty(\tau, h)$	C-Order	h^{-1}	$E_\infty(\tau, h)$	C-Order	h^{-1}	$E_\infty(\tau, h)$	C-Order
6	3.1728E-03	–	6	3.0484E-03	–	6	2.8848E-03	–
10	1.2360E-03	1.8455	10	1.1921E-03	1.8380	10	1.1312E-03	1.8327
14	6.4392E-04	1.9379	14	6.2047E-04	1.9407	14	5.8594E-04	1.9550
18	3.9126E-04	1.9824	18	3.7721E-04	1.9803	18	3.5494E-04	1.9946

can be seen that the FEG and MFEG methods result in simulations with rapid convergence and fewer iterations in comparison to the C-N difference scheme. Among the presented schemes, the MFEG method is clearly the fastest one since it uses the least amount of time consumption for simulating the test problems. The numerical errors and convergence orders of the MFEG method are reported in Table 12. The results are in good agreement with the theoretical analysis.

Conclusion

In the current work, we presented the FEG method and the MFEG method, which are derived based on the combination of two C-N difference schemes with grouping strategies on the standard grid to solve the two-dimensional time fractional mobile/immobile equation. The Fourier analysis method is utilized to prove the stability and convergence in l^2 norm. A comparison of the FEG and MFEG methods with the C-N difference scheme is given in terms of computational time, iterations' number and maximum error. The computational orders of the proposed methods are calculated and found to be in good agreement with the theoretical analysis. Numerical experiments showed that the exact solutions are well matched using all the tested methods. Furthermore, experimental results verified that the FEG and MFEG methods outperform the C-N difference scheme in terms of iterations' number and execution time, showing their efficiency. Overall, the proposed methods have the advantages of being accurate, computationally efficient and applicable to other types of linear and nonlinear multi-dimensional fractional problems. As an outlook for future, the parallel implementation technique is fairly meaningful to enhance the computational efficiency of the developed methods.

Author Contributions All authors have read and approved the current version of the manuscript.

Funding This work received no external funding.

Availability of data and materials All data generated or analysed during this study are included in this published article.

Declarations

Conflict of interest On behalf of all authors, the corresponding author states that there is no conflict of interest.

Code availability All numerical simulations have been conducted using Matlab R2018b.

References

1. Milici, C., Drăgănescu, G., Machado, J.T.: Introduction to Fractional Differential Equations, vol. 25. Springer, Switzerland (2018)
2. Owolabi, K.M., Atangana, A.: Numerical Methods for Fractional Differentiation. Springer, Singapore (2019)
3. Atangana, A.: Fractional Operators with Constant and Variable Order with Application to Geo-hydrology. Academic Press, New York (2017)
4. Tarasov, V.E.: Handbook of Fractional Calculus with Applications vol. 3-8. de Gruyter, Boston (2019)
5. Dutta, H., Akdemir, A.O., Atangana, A.: Fractional Order Analysis: Theory. Methods and Applications. John Wiley & Sons, Hoboken (2020)
6. Viera-Martin, E., Gómez-Aguilar, J., Solís-Pérez, J., Hernández-Pérez, J., Escobar-Jiménez, R.: Artificial neural networks: a practical review of applications involving fractional calculus. The European Physical Journal Special Topics, 1–37 (2022)
7. Hassouna, M., Ouhadan, A., et al.: Fractional calculus: applications in rheology. In: Fractional Order Systems, 513–549. Elsevier, ??? (2022)
8. Barros, LCd., Lopes, M.M., Pedro, F.S., Esmi, E., Santos, J.PCd., Sánchez, D.E.: The memory effect on fractional calculus: an application in the spread of covid-19. Comput. Appl. Math. **40**(3), 1–21 (2021)
9. Atangana, A., Baleanu, D.: Caputo-fabrizio derivative applied to groundwater flow within confined aquifer. J. Eng. Mech. **143**(5), 4016005 (2017)
10. Atangana, A., Gómez-Aguilar, J.: Fractional derivatives with no-index law property: application to chaos and statistics. Chaos, Solitons & Fractals **114**, 516–535 (2018)

11. Sun, H., Zhang, Y., Baleanu, D., Chen, W., Chen, Y.: A new collection of real world applications of fractional calculus in science and engineering. Commun. Nonlinear Sci. Numer. Simul. **64**, 213–231 (2018)
12. Zhang, X., Li, R., Hong, J., Zhou, X., Xin, N., Li, Q.: Image-enhanced single-pixel imaging using fractional calculus. Opt. Express **30**(1), 81–91 (2022)
13. Aman, S., Khan, I., Ismail, Z., Salleh, M.Z.: Applications of fractional derivatives to nanofluids: exact and numerical solutions. Mathematical Modelling of Natural Phenomena **13**(1), 2 (2018)
14. Khan, I., Shah, N.A., Mahsud, Y., Vieru, D.: Heat transfer analysis in a maxwell fluid over an oscillating vertical plate using fractional caputo-fabrizio derivatives. The European Physical Journal Plus **132**(4), 1–12 (2017)
15. Almeida, R., Malinowska, A.B., Monteiro, M.T.T.: Fractional differential equations with a caputo derivative with respect to a kernel function and their applications. Mathematical Methods in the Applied Sciences **41**(1), 336–352 (2018)
16. Alshabanat, A., Jleli, M., Kumar, S., Samet, B.: Generalization of caputo-fabrizio fractional derivative and applications to electrical circuits. Frontiers in Physics **8**, 64 (2020)
17. Ali, F., Murtaza, S., Khan, I., Sheikh, N.A., Nisar, K.S.: Atangana-baleanu fractional model for the flow of jeffrey nanofluid with diffusion-thermo effects: Applications in engine oil. Adv. Difference Equ. **2019**(1), 1–21 (2019)
18. Gao, W., Ghanbari, B., Baskonus, H.M.: New numerical simulations for some real world problems with atangana-baleanu fractional derivative. Chaos, Solitons & Fractals **128**, 34–43 (2019)
19. Uçar, S., Uçar, E., Özdemir, N., Hammouch, Z.: Mathematical analysis and numerical simulation for a smoking model with atangana-baleanu derivative. Chaos, Solitons & Fractals **118**, 300–306 (2019)
20. Alrabaiah, H., Zeb, A., Alzahrani, E., Shah, K.: Dynamical analysis of fractional-order tobacco smoking model containing snuffing class. Alex. Eng. J. **60**(4), 3669–3678 (2021)
21. Ndaïrou, F., Area, I., Nieto, J.J., Silva, C.J., Torres, D.F.: Fractional model of covid-19 applied to galicia, spain and portugal. Chaos, Solitons & Fractals **144**, 110652 (2021)
22. Chávez-Vázquez, S., Gómez-Aguilar, J.F., Lavín-Delgado, J., Escobar-Jiménez, R.F., Olivares-Peregrino, V.H.: Applications of fractional operators in robotics: a review. Journal of Intelligent & Robotic Systems **104**(4), 1–40 (2022)
23. Zhang, Y., Sun, H., Stowell, H.H., Zayernouri, M., Hansen, S.E.: A review of applications of fractional calculus in earth system dynamics. Chaos, Solitons & Fractals **102**, 29–46 (2017)
24. Chu, Y.-M., Bekiros, S., Zambrano-Serrano, E., Orozco-López, O., Lahmiri, S., Jahanshahi, H., Aly, A.A.: Artificial macro-economics: A chaotic discrete-time fractional-order laboratory model. Chaos, Solitons & Fractals **145**, 110776 (2021)
25. Tarasova, V.V., Tarasov, V.E.: Economic interpretation of fractional derivatives. Prog. Fractional Differ. Appl. **3**, 1–17 (2017)
26. Yang, X., Zhang, H., Tang, Q.: A spline collocation method for a fractional mobile-immobile equation with variable coefficients. Comput. Appl. Math. **39**(1), 1–20 (2020)
27. Liu, Z., Li, X.: A crank-nicolson difference scheme for the time variable fractional mobile-immobile advection-dispersion equation. J. Appl. Math. Comput. **56**(1), 391–410 (2018)
28. Pourbashash, H., Baleanu, D., Al Qurashi, M.M.: On solving fractional mobile/immobile equation. Adv. Mech. Eng. **9**(1), 1687814016688616 (2017)
29. Qiu, W., Xu, D., Guo, J., Zhou, J.: A time two-grid algorithm based on finite difference method for the two-dimensional nonlinear time-fractional mobile/immobile transport model. Numerical Algorithms **85**(1), 39–58 (2020)
30. Jiang, H., Xu, D., Qiu, W., Zhou, J.: An adi compact difference scheme for the two-dimensional semilinear time-fractional mobile-immobile equation. Comput. Appl. Math. **39**(4), 1–17 (2020)
31. Yin, B., Liu, Y., Li, H.: A class of shifted high-order numerical methods for the fractional mobile/immobile transport equations. Appl. Math. Comput. **368**, 124799 (2020)
32. Chai, L., Liu, Y., Li, H.: Fourth-order compact difference schemes for the two-dimensional nonlinear fractional mobile/immobile transport models. Computers & Mathematics with Applications **100**, 1–10 (2021)
33. Sunarto, A., Agarwal, P., Sulaiman, J., Chew, J.V.L., Momani, S.: Quarter-sweep preconditioned relaxation method, algorithm and efficiency analysis for fractional mathematical equation. Fractal and Fractional **5**(3), 98 (2021)
34. Salama, F.M., Abd Hamid, N.N., Ali, N.H.M.: Fast O(N) hybrid laplace transform-finite difference method in solving 2d time fractional diffusion equation. Journal of Mathematics and Computer Science **23**(2), 110–123 (2021)
35. Saeed, A.M., AL-harbi, N.M.: Group splitting with sor/aor methods for solving boundary value problems: A computational comparison. European Journal of Pure and Applied Mathematics **14**(3), 905–914 (2021)

36. Salama, F.M., Ali, N.H.M.: Computationally efficient hybrid method for the numerical solution of the 2D time fractional advection-diffusion equation. International Journal of Mathematical, Engineering and Management Sciences **5**(3), 432–446 (2020)
37. Salama, F.M., Abd Hamid, N.N., Ali, N.H.M.: Efficient hybrid group iterative methods in the solution of two-dimensional time fractional cable equation. Adv. Difference Equ. **2020**(1), 1–20 (2020)
38. Abdi, N., Aminikhah, H., Sheikhani, A., Alavi, J., Taghipour, M.: An efficient explicit decoupled group method for solving two–dimensional fractional burgers' equation and its convergence analysis. Advances in Mathematical Physics **2021**, (2021)
39. Abdi, N., Aminikhah, H., Sheikhani, A.R.: High-order rotated grid point iterative method for solving 2d time fractional telegraph equation and its convergence analysis. Comput. Appl. Math. **40**(2), 1–26 (2021)
40. Khan, M.A., Ali, N.H.M., Abd Hamid, N.N.: A new fourth-order explicit group method in the solution of two-dimensional fractional rayleigh-stokes problem for a heated generalized second-grade fluid. Adv. Difference Equ. **2020**(1), 1–22 (2020)
41. Khan, M.A., Ali, N.H.M., Abd Hamid, N.N.: The design of new high-order group iterative method in the solution of two-dimensional fractional cable equation. Alex. Eng. J. **60**(4), 3553–3563 (2021)
42. Ali, A., Abdeljawad, T., Iqbal, A., Akram, T., Abbas, M.: On unconditionally stable new modified fractional group iterative scheme for the solution of 2d time-fractional telegraph model. Symmetry **13**(11), 2078 (2021)
43. Salama, F.M., Abd Hamid, N.N., Ali, N.H.M., Ali, U.: An efficient modified hybrid explicit group iterative method for the time-fractional diffusion equation in two space dimensions. AIMS Mathematics **7**(2), 2370–2392 (2022)
44. Salama, F.M., Abd Hamid, N.N., Ali, U., Ali, N.H.M.: Fast hybrid explicit group methods for solving 2d fractional advection-diffusion equation. AIMS Mathematics **7**(9), 15854–15880 (2022)
45. Modanlı, M.: Two numerical methods for fractional partial differential equation with nonlocal boundary value problem. Adv. Difference Equ. **2018**(1), 1–19 (2018)
46. Karatay, I., Kale, N., Bayramoglu, S.: A new difference scheme for time fractional heat equations based on the crank-nicholson method. Fractional Calculus and Applied Analysis **16**(4), 892–910 (2013)
47. Abbaszadeh, M., Amjadian, H.: Second-order finite difference/spectral element formulation for solving the fractional advection-diffusion equation. Communications on Applied Mathematics and Computation, 1–17 (2020)